Adaptive Target Detection and DOA Estimation With Uniform Rectangular Arrays in the Presence of Unknown Mutual Coupling

Lan Lan, *Member, IEEE*, Massimo Rosamilia, *Member, IEEE*, Augusto Aubry, *Senior Member, IEEE*, Antonio De Maio, *Fellow, IEEE*, and Guisheng Liao, *Senior Member, IEEE*

***Abstract*— This paper investigates joint adaptive target detection and direction of arrival (DOA) estimation via a uniform rectangular array (URA) affected by mutual coupling. Capitalizing on a bespoke linearization of the array manifold and leveraging the banded symmetric Toeplitz block Toeplitz structure for the coupling matrix description, a vectorial model of the useful target echo return is proposed and used to formulate the detection problem. Two decision rules are designed, i.e., the generalized likelihood ratio (GLR) and multifamily likelihood ratio test (MFLRT), with the latter aimed at handling an unknown number of active mutual coupling coefficients. Both demand the joint maximum likelihood (ML) estimates of the coupling coefficients and the target angular displacement parameters which can be obtained solving a non-convex optimization problem. Toward this goal, an iterative procedure based on the minorization-maximization (MM) algorithm is developed. At the analysis stage, the performance of the proposed methods is assessed in terms of detection probability (P_d) and DOA root mean square error (RMSE) in comparison with benchmarks and standard strategies that do not account for the mutual coupling phenomenon. The results demonstrate the effectiveness of the proposed approaches to overcome signal mismatches induced by both the DOA uncertainty and mutual coupling.**

***Index Terms*— Adaptive radar detection, mutual coupling, uniform rectangular arrays, GLRT, MFLRT.**

Manuscript received 15 February 2023; revised 25 April 2023; accepted 11 June 2023. Date of publication 27 June 2023; date of current version 15 August 2023. The work of Lan Lan was supported in part by the National Natural Science Foundation of China under Grant 62101402 and Grant 61931016, in part by the China Postdoctoral Science Foundation under Grant 2021TQ0261 and Grant 2021M702547, in part by the Shanghai Academy of Spaceflight Technology (SAST) Innovation Fund under Grant SAST2022-041, and in part by the Science and Technology Innovation Team of Shaanxi Province under Grant 2022TD-38. The work of Augusto Aubry and Antonio De Maio was supported by the European Union under the Italian National Recovery and Resilience Plan (NRRP) of NextGenerationEU, partnership on "Telecommunications of the Future" (CUP J33C22002880001, PE00000001 - program "RESTART"). *(Corresponding author: Antonio De Maio.)*

Lan Lan and Guisheng Liao are with the National Key Laboratory of Radar Signal Processing, Xidian University, Xi'an 710071, China (e-mail: lanlan@xidian.edu.cn; liaogs@xidian.edu.cn).

Massimo Rosamilia is with the National Inter-University Consortium for Telecommunications, 43124 Parma, Italy (e-mail: massimo.rosamilia@unina.it).

Augusto Aubry and Antonio De Maio are with the Department of Electrical Engineering and Information Technologies (DIETI), University of Naples Federico II, 80125 Naples, Italy, and also with the National Inter-University Consortium for Telecommunications, 43124 Parma, Italy (e-mail: augusto.aubry@unina.it; ademaio@unina.it).

Digital Object Identifier 10.1109/TRS.2023.3289991

I. Introduction

AMONG the several challenges that modern antenna array signal processing algorithms [1] are faced with, the presence of mutual coupling (MC) is definitely a very crucial issue [2], [3], [4], [5], [6], [7]. In fact, elements of an antenna array may electromagnetically interact with their neighbors, altering their electromagnetic characteristics. This unwanted effect depends on a multitude of factors, including the number, type, and relative orientation of each antenna element, as well as their distance and position [5], [8], [9]. As a result, the actual received steering vector could be possibly mismatched with respect to (w.r.t.) the ideal manifold model assumed at the design stage by standard algorithms, eventually causing a significant performance degradation [2], [10], [11], [12], [13]. Despite of the potential measurement campaigns to quantify and compensate accurately the MC, some residual effects due to an unavoidable imperfect measurements are often present. Moreover, the MC effect is not necessarily stationary [2], making it challenging to keep the array properly calibrated over time. In this regard, a frequent calibration process to ensure optimal performance is time-consuming and complex, effectively wasting valuable radar time. Therefore, it is crucial to investigate adaptive signal processing methods capable of realizing an on-the-fly compensation of the MC (or its residual, if a initial calibration stage has been performed).

An interesting aspect of MC is that the magnitude of the coupling coefficient describing the interaction between two radiating elements decreases rapidly with the distance between them, and it is substantially the same between any two elements that are at the same distance [8]. This property, together with special symmetries induced by the array geometrical configuration, yields a special structure in the MC matrix (MCM) which can be capitalized at the design stage of bespoke signal processing schemes [2], [14], [15], [16], [17], [18].

To proceed further, let us now frame the aforementioned issue within a typical radar context, with emphasis on adaptive target detection [19], [20], [21], [22], [23], [24] and direction of arrival (DOA) estimation [25], [26], [27], [28]. In [13], assuming a uniform linear array (ULA) affected by MC, the problem of jointly detecting the target and estimating its bearing is addressed while accounting for MC and the DOA uncertainty along the design phase. This is achieved

by modeling the actual steering vector as the product of a MCM and an approximated steering vector depending affinely on the unknown DOA displacement (w.r.t. the looking direction) [29]. The target detection problem, formulated assuming a homogeneous radar interference environment, is addressed by resorting to the generalized likelihood ratio test (GLRT) [30], [31] and the multifamily likelihood ratio test (MFLRT) [32] strategies, with the latter employed when an *a-priori* knowledge on the number of active mutual coupling coefficients is unavailable (also referred to as the unknown model order case).

Following the guidelines of [13], this work aims at simultaneously detecting and estimating the two-dimensional (2D) DOA with a uniform rectangular array (URA) in the presence of MC. Specifically, the main innovative technical achievements as compared to [13] can be summarized as follows:

- For URA, the MCM demands a different structural model w.r.t. the ULA case. Specifically, a banded symmetric Toeplitz block Toeplitz MCM [18] is necessary instead of the banded symmetric Toeplitz matrix used for the ULA. From the analytic viewpoint this involves different numbers of parameters to estimate and tailored matrix manipulations to capitalize on the developed matrix model.
- After an appropriate concentration of likelihood functions exploiting the estimates of the interference-plus-noise covariance matrix and the MC coefficients, to handle the joint detection and estimation problem for the URA case it is required the solution of a two-dimensional optimization problem, unlike the ULA sensing scenario [13] involving a one-dimensional problem. The subsequent application of the minorization-maximization (MM) optimization framework for the URA entails solving, at each iteration, a new two-variable box-constrained quadratic optimization problem, wherein its optimal solution is provided in closed form.
- For the URA configuration, the performance of the devised methods is numerically assessed in terms of probability of detection (P_d) and root mean square error (RMSE) of the 2D DOA estimates, via Monte Carlo simulations. The results are also compared with benchmarks and counterparts available in the open literature. In addition, a robustness analysis is conducted to evaluate the effectiveness of the proposed strategies in case of mismatches in the MC model, namely when the actual MCM does not fully exhibit the banded symmetric Toeplitz block Toeplitz structure assumed at the design stage.

The paper is organized as follows. The signal model for URA with MC effect is given in Section II. In Section III, the design of decision statistics and parameters estimation processes for known and unknown model order cases are addressed. Numerical simulations are provided in Section IV. Finally, conclusions as well as future research activities are discussed in Section V.

A. Notations

Boldface is used for vectors $\boldsymbol{a}$ (lower case), and matrices $\boldsymbol{A}$ (upper case). The (k,l)-entry (or l-entry) of a generic matrix $\boldsymbol{A}$ (or vector $\boldsymbol{a}$) is indicated as $[\boldsymbol{A}]_{k,l}$ (or $[\boldsymbol{a}]_l$). $\boldsymbol{I}$ and $\boldsymbol{0}$ denote respectively the identity matrix and the matrix with zero entries (their size is determined from the context). Moreover, $\mathrm{diag}(\boldsymbol{x})$ indicates the diagonal matrix whose i-th diagonal element is $[\boldsymbol{x}]_i$. The transpose and the conjugate transpose operators are denoted by the symbols $(\cdot)^{\mathrm{T}}$ and $(\cdot)^{\dagger}$, respectively. The determinant and the trace of the matrix $\boldsymbol{A} \in \mathbb{C}^{N\times N}$ are indicated with $|\boldsymbol{A}|$, $\mathrm{tr}\{\boldsymbol{A}\}$, respectively. $\otimes$ denotes the Kronecker product. $\mathbb{R}^N$ and $\mathbb{C}^N$ are the sets of N-dimensional column vectors of real and complex numbers, respectively. $\mathbb{H}^N$ and $\mathbb{H}^N_{++}$ represent the set of $N \times N$ Hermitian matrices and Hermitian positive definite matrices, respectively. The letter j represents the imaginary unit (i.e., $j = \sqrt{-1}$). For any complex number x, $|x|$ indicates the modulus of x and $\mathrm{Re}\{x\}$ denotes its real part. Moreover, for any $\boldsymbol{x} \in \mathbb{C}^N$, $\|\boldsymbol{x}\|$ denotes the Euclidean norm, whereas the Frobenius norm of a matrix $\boldsymbol{A}$ is indicated as $\|\boldsymbol{A}\|_F$. Let $f(\boldsymbol{x})$ be a real-valued function, $\nabla_{\boldsymbol{x}} f(\boldsymbol{x})$ denotes the gradient of $f(\cdot)$ w.r.t. $\boldsymbol{x}$, with the partial derivatives arranged in a column vector. Furthermore, for any $x, y \in \mathbb{R}$, $\max(x, y)$ returns the maximum between the two argument values. Finally, the symbol $\mathcal{O}(\cdot)$ denotes the computational complexity in terms of basic operations.

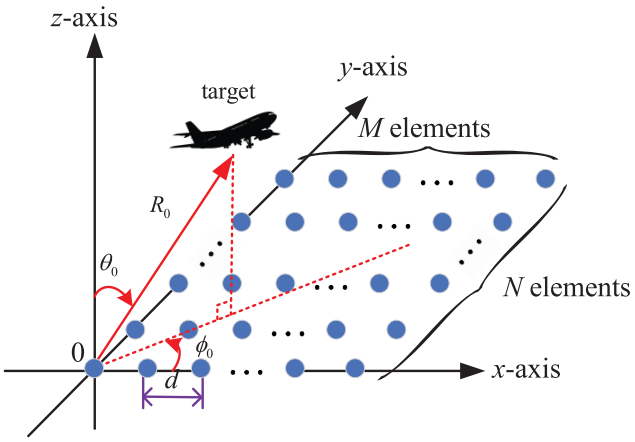

Fig. 1. System configuration of a URA having $M \times N$ elements arranged in the xoy-plane.

II. Signal Model

A. Signal Model With Unknown MC

Let us consider a radar system equipped with a URA consisting of $M \times N$ antenna elements on the xy-plane with inter-element spacing equal to d (see Fig. 1).

Assume that a point-like target is located in the far-field with the range R_0, azimuth ϕ_0, and elevation θ_0. The radar received echo after down-conversion, pulse compression, fast-time sampling, and measurement gathering at the instant of interest, is given by

$$a\,\boldsymbol{p}(u_0, v_0) = a\,\boldsymbol{p}_u(u_0) \otimes \boldsymbol{p}_v(v_0), \tag{1}$$

where $a \in \mathbb{C}$ denotes the unknown complex coefficient accounting for target backscattering as well as the other terms involved in the two-way radar equation, $\boldsymbol{p}(u_0, v_0) = \boldsymbol{p}_u(u_0) \otimes \boldsymbol{p}_v(v_0) \in \mathbb{C}^{MN}$ is the 2D spatial steering vector

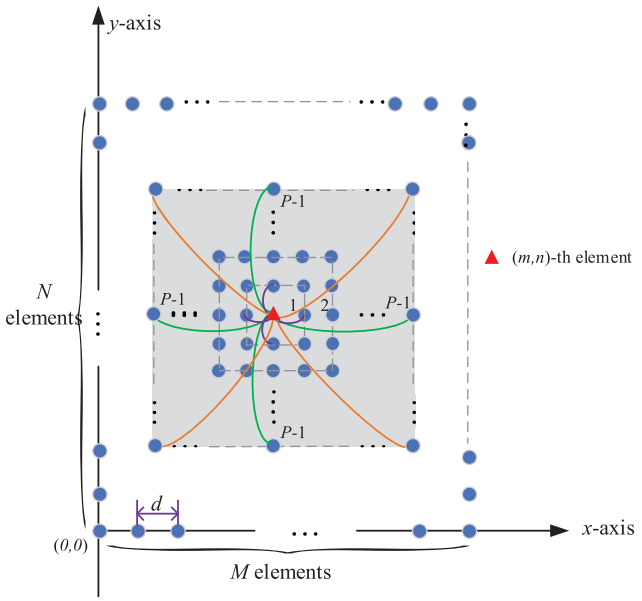

Fig. 2. Representation of the MC in a URA between the (m, n)-th antenna element and its $4P(P-1)$ nearest elements.

$\boldsymbol{p}(u, v)$ evaluated at (u_0, v_0), with $u_0 = \cos(\phi_0)\sin(\theta_0)$ and $v_0 = \sin(\phi_0)\sin(\theta_0)$ the target location parameters in the space of directional cosines [22], and

$$\boldsymbol{p}_u(u) = \left[1, e^{j2\pi\frac{d}{\lambda_0}u}, \ldots, e^{j2\pi\frac{d}{\lambda_0}(M-1)u}\right]^{\mathrm{T}} \in \mathbb{C}^M \tag{2}$$

$$\boldsymbol{p}_v(v) = \left[1, e^{j2\pi\frac{d}{\lambda_0}v}, \ldots, e^{j2\pi\frac{d}{\lambda_0}(N-1)v}\right]^{\mathrm{T}} \in \mathbb{C}^N \tag{3}$$

the spatial steering vectors pertaining to the u and v domains, respectively.

Up to now, an ideal array manifold has been considered. In practice, the MC phenomenon within the array elements is almost unavoidable and demands a bespoke description at the modeling stage so as to be appropriately handled at the information extraction level. Therefore, the coupling effects can be accounted for by representing the actual steering vector as

$$\boldsymbol{p}_m(u_0, v_0) = \boldsymbol{C}\,\boldsymbol{p}(u_0, v_0), \tag{4}$$

where $\boldsymbol{C} \in \mathbb{C}^{MN\times MN}$ is the MCM.

To effectively model $\boldsymbol{C}$, it is assumed that the MC between any pair of elements at the same distance is essentially the same,[1] whereas it decreases rapidly as their distance increases. Moreover, it can be practically ignored for elements fairly separated in distance from each other [8]. Recently, this standard MCM model, originally developed for linear and circular arrays [2], [15], [16], [17], [33], [34], [35], has been extended to the planar array case [18]. Thereby, assuming that for each radiating element the MC effect is induced only by elements within a specific grid/neighborhood around it [18], $P-1$ outgrowing squares could be conceived (see Fig. 2 where different colors represent distinct geometric symmetries in the electromagnetic field leakage), resulting in a total of $4P(P-1)$ nearest elements mutually coupled with the (m, n)-th ($m = 1, \ldots, M$, $n = 1, \ldots, N$) element. Accordingly, the MCM is represented accurately as a banded symmetric Toeplitz block Toeplitz matrix [36], whereby each block, denoted by $\boldsymbol{C}_i \in \mathbb{C}^{N\times N}$, describes the intercolumn and intracolumn MC for $i = 1$ and $i \geq 2$, respectively, experienced by the elements of one column of the URA induced by those lying in the $(i-1)$-th adjacent column, if present. Therefore, each matrix block is a banded symmetric Toeplitz matrix. Formally,

$$\boldsymbol{C} = \begin{bmatrix} \boldsymbol{C}_1 & \boldsymbol{C}_2 & \cdots & \boldsymbol{C}_P & \boldsymbol{0} & \cdots & \cdots & \cdots & \boldsymbol{0} \\ \boldsymbol{C}_2 & \boldsymbol{C}_1 & \boldsymbol{C}_2 & \cdots & \boldsymbol{C}_P & \boldsymbol{0} & \cdots & \cdots & \boldsymbol{0} \\ \vdots & \ddots & \ddots & \ddots & \ddots & \ddots & \ddots & \ddots & \vdots \\ \boldsymbol{C}_P & \cdots & \boldsymbol{C}_2 & \boldsymbol{C}_1 & \boldsymbol{C}_2 & \cdots & \boldsymbol{C}_P & \cdots & \boldsymbol{0} \\ \boldsymbol{0} & \ddots & \ddots & \ddots & \ddots & \ddots & \ddots & \ddots & \vdots \\ \vdots & \ddots & \boldsymbol{C}_P & \cdots & \boldsymbol{C}_2 & \boldsymbol{C}_1 & \boldsymbol{C}_2 & \cdots & \boldsymbol{C}_P \\ \vdots & \ddots & \ddots & \ddots & \ddots & \ddots & \ddots & \ddots & \vdots \\ \boldsymbol{0} & \cdots & \cdots & \boldsymbol{0} & \boldsymbol{C}_P & \cdots & \boldsymbol{C}_2 & \boldsymbol{C}_1 & \boldsymbol{C}_2 \\ \boldsymbol{0} & \cdots & \cdots & \cdots & \boldsymbol{0} & \boldsymbol{C}_P & \cdots & \boldsymbol{C}_2 & \boldsymbol{C}_1 \end{bmatrix}, \tag{5}$$

where

$$\begin{aligned} \boldsymbol{C}_i &= \begin{bmatrix} [\boldsymbol{c}_i]_1 & [\boldsymbol{c}_i]_2 & \cdots & [\boldsymbol{c}_i]_P & \cdots & 0 \\ [\boldsymbol{c}_i]_2 & [\boldsymbol{c}_i]_1 & [\boldsymbol{c}_i]_2 & \cdots & \ddots & \vdots \\ \vdots & [\boldsymbol{c}_i]_2 & [\boldsymbol{c}_i]_1 & \ddots & \cdots & [\boldsymbol{c}_i]_P \\ [\boldsymbol{c}_i]_P & \cdots & \ddots & \ddots & [\boldsymbol{c}_i]_2 & \vdots \\ \vdots & \ddots & & [\boldsymbol{c}_i]_2 & [\boldsymbol{c}_i]_1 & [\boldsymbol{c}_i]_2 \\ 0 & \cdots & [\boldsymbol{c}_i]_P & \cdots & [\boldsymbol{c}_i]_2 & [\boldsymbol{c}_i]_1 \end{bmatrix} \\ &= [\boldsymbol{c}_i]_1 \boldsymbol{I}_N + \sum_{m=1}^{P-1} [\boldsymbol{c}_{i+1}]_m \boldsymbol{J}_m, \end{aligned} \tag{6}$$

is in one-to-one mapping with $\boldsymbol{c}_i = [[\boldsymbol{c}_i]_1, [\boldsymbol{c}_i]_2, \ldots, [\boldsymbol{c}_i]_P]^{\mathrm{T}} \in \mathbb{C}^P$, $i = 1, 2, \ldots, P$, whereas $\boldsymbol{J}_m$ is defined as an $N \times N$ matrix having 1s on its m-th ($m = 1, 2, \ldots, P-1$) upper and lower diagonals, and zeros otherwise, i.e.,

$$[\boldsymbol{J}_m]_{p,q} = \begin{cases} 1, & |p-q| = m \\ 0, & otherwise \end{cases}, \quad p, q = 1, \ldots, N. \tag{7}$$

It is interesting to observe that when the Toeplitz-block-Toeplitz matric $\boldsymbol{C}$ (5) can be factored as $\boldsymbol{C}_u \otimes \boldsymbol{C}_v$ (with $\boldsymbol{C}_u$ and $\boldsymbol{C}_v$ banded Toeplitz matrices), multiplying $\boldsymbol{C}$ by the steering vector (4), yields $\boldsymbol{C}\,\boldsymbol{p} = \boldsymbol{C}_u \boldsymbol{p}_u \otimes \boldsymbol{C}_v \boldsymbol{p}_v$, which is analytically equivalent to the factored model used in [37] and [38] for Multiple Input Multiple Output (MIMO) systems.

Exploiting the structural features of the overall MCM, i.e., $\boldsymbol{C}$, it can be further decomposed as

$$\boldsymbol{C} = \boldsymbol{I}_M \otimes \boldsymbol{C}_1 + \sum_{i=1}^{P-1} \boldsymbol{D}_i \otimes \boldsymbol{C}_{i+1} = \sum_{i=0}^{P-1} \boldsymbol{D}_i \otimes \boldsymbol{C}_{i+1}, \tag{8}$$

with $\boldsymbol{D}_0 = \boldsymbol{I}_M$ and $\boldsymbol{D}_i \in \mathbb{C}^{M\times M}$, $i = 1, \ldots, P-1$, a matrix having 1s on its i-th upper and lower diagonals, and zeros otherwise.

[1]Notice that the assumption is realistic for modern phased array radar systems with plenty of elements. Specifically, it reasonably holds true for internal elements but could not be ensured for those close or exactly on to the edges [5].

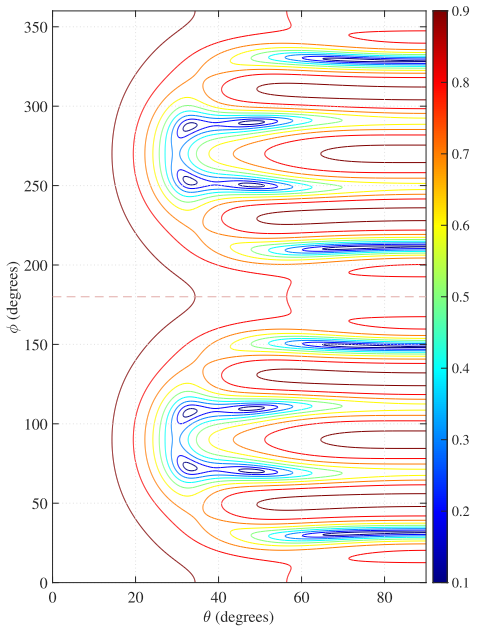

Fig. 3. Cosine similarity (9) between the ideal and the actual steering vectors.

To further assess the influence of the MC effect, in the following the angle cosine (cosine similarity) [39] between the ideal and the actual steering vectors is analyzed, by means of

$$\cos_m(u, v) = \frac{|\boldsymbol{p}_m^{\dagger}(u, v)\boldsymbol{p}(u, v)|}{\|\boldsymbol{p}_m(u, v)\|\|\boldsymbol{p}(u, v)\|}. \tag{9}$$

As a study case, let us consider a URA with $M = 5$ and $N = 6$ experiencing the MC phenomenon, which is modeled assuming $P = 3$, with the matrices $\boldsymbol{C}_1$, $\boldsymbol{C}_2$, and $\boldsymbol{C}_3$ defined as in (6) using the following vectors $\boldsymbol{c}_1 = [1, 0.75+0.48j, 0.67+0.32j]^{\mathrm{T}}$, $\boldsymbol{c}_2 = [0.58+0.29j, 0.42-0.35j, 0.39+0.24j]^{\mathrm{T}}$, and $\boldsymbol{c}_3 = [0.03+0.45j, 0.12-0.31j, 0.09-0.18j]^{\mathrm{T}}$, respectively. In Fig. 3, (9) is plotted versus θ and ϕ. Its inspection highlights that a symmetric response is obtained w.r.t. $\phi = 180°$. Moreover, in some regions the mismatch induced by the MC is quite severe. This is for example the case of $(\theta, \phi) \in [30°, 55°] \times [65, 75]$. In such instances, there is a strong mismatch between the actual and the ideal model as testified by the considerable low values of the cosine similarity.

B. Signal Model via Linearized Array Manifold

Following the guidelines of [29], the ideal received steering vector $\boldsymbol{p}(u, v)$ can be approximated via a first order Taylor expansion around the pointing direction $(\bar{u}, \bar{v})$ with a resulting functional dependency of the linearized array manifold on the offsets $\Delta u = u_0 - \bar{u}$ and $\Delta v = v_0 - \bar{v}$, namely

$$\boldsymbol{p}(u_0, v_0) \approx \boldsymbol{p}_a(\Delta u, \Delta v) = \boldsymbol{p} + \hat{\boldsymbol{p}}_u \Delta u + \hat{\boldsymbol{p}}_v \Delta v, \tag{10}$$

where $\boldsymbol{p} = \boldsymbol{p}(\bar{u}, \bar{v})$, $\hat{\boldsymbol{p}}_v = \dot{\boldsymbol{p}}_u \otimes \boldsymbol{p}_v(\bar{v})$, and $\hat{\boldsymbol{p}}_v = \boldsymbol{p}_u(\bar{u}) \otimes \dot{\boldsymbol{p}}_v$ with $\dot{\boldsymbol{p}}_u$ and $\dot{\boldsymbol{p}}_v$ the vectors whose entries contain the derivative of $\boldsymbol{p}_u$ and $\boldsymbol{p}_v$ w.r.t. u and v evaluated at $\bar{u}$ and $\bar{v}$, respectively (See Appendix A).

Now, letting $\boldsymbol{p}_u = \boldsymbol{p}_u(\bar{u})$, $\boldsymbol{p}_v = \boldsymbol{p}_v(\bar{u})$, and including the coupling effects, the echo signal can be expressed as

$$\begin{aligned} a\boldsymbol{p}_{am}(\Delta u, \Delta v) &= a\boldsymbol{C}\boldsymbol{p}_a(\Delta u, \Delta v) = \boldsymbol{B}\boldsymbol{p}_a(\Delta u, \Delta v) \\ &= \boldsymbol{H}(\Delta u, \Delta v)\boldsymbol{b}, \end{aligned} \tag{11}$$

with $\boldsymbol{p}_{am}(\Delta u, \Delta v) = \boldsymbol{C}\boldsymbol{p}_a(\Delta u, \Delta v) \in \mathbb{C}^{MN}$ the approximated actual steering vector encompassing the MC effect, $\boldsymbol{B} = a\boldsymbol{C} = \sum_{i=0}^{P-1} \boldsymbol{D}_i \otimes a\boldsymbol{C}_{i+1} \in \mathbb{C}^{MN \times MN}$, whereas the specific definitions of $\boldsymbol{H}(\Delta u, \Delta v) \in \mathbb{C}^{MN \times P^2}$ and $\boldsymbol{b} \in \mathbb{C}^{P^2}$ are provided in Appendix B.

Before concluding this section, it is worth mentioning that following the same line of reasoning of [13], it can be shown that a sufficient condition for the identifiability of the unknowns in (11) is given by $MN \geq 3P^2$, namely $\boldsymbol{H}_1 = \left[\boldsymbol{H}_0, \tilde{\boldsymbol{H}}, \hat{\boldsymbol{H}}\right] \in \mathbb{C}^{MN \times 3P^2}$ being full rank.

III. Target Detection Problem

The target detection problem is formulated as a binary hypothesis test aimed at ascertaining the target presence/absence within the cell under test. Assuming the availability of K secondary data free of any useful target signal (with $K > MN$), it can be cast as

$$\begin{cases} \mathcal{H}_0 : \begin{cases} \boldsymbol{r} = \boldsymbol{n} \\ \boldsymbol{r}_k = \boldsymbol{n}_k, \quad k = 1, \ldots, K \end{cases} \\ \mathcal{H}_1 : \begin{cases} \boldsymbol{r} = \boldsymbol{H}(\Delta u, \Delta v)\boldsymbol{b} + \boldsymbol{n} \\ \boldsymbol{r}_k = \boldsymbol{n}_k, \quad k = 1, \ldots, K \end{cases} \end{cases}, \tag{12}$$

where

- $\boldsymbol{r} \in \mathbb{C}^{MN}$ and $\boldsymbol{r}_k \in \mathbb{C}^{MN}, k = 1, \ldots, K$, are the vectors of primary and secondary data, respectively;
- $\boldsymbol{H}(\Delta u, \Delta v)$ is functionally dependent on the unknown target DOA displacements w.r.t. the array pointing direction;
- $\boldsymbol{b}$ represents the unknown vector accounting for both the complex received target echo return a and the P^2 complex MC coefficients;
- $\boldsymbol{n} \in \mathbb{C}^{MN}$ and $\boldsymbol{n}_k \in \mathbb{C}^{MN}$, $k = 1, \ldots, K$, denote the interference plus noise components of the received snapshots, modeled as statistically independent, complex, zero-mean, circularly symmetric Gaussian random vectors with unknown positive definite covariance matrix, i.e., $\boldsymbol{M} = E[\boldsymbol{n}\boldsymbol{n}^{\dagger}] = E[\boldsymbol{n}_k\boldsymbol{n}_k^{\dagger}] \in \mathbb{H}_{++}^{MN}, k = 1, \ldots, K$.

Accordingly, the joint probability density functions (PDFs) of the observations under $\mathcal{H}_0$ and $\mathcal{H}_1$, can be written respectively as

$$\begin{aligned} &f_{\mathcal{H}_i}(\boldsymbol{r}, \boldsymbol{r}_1, \ldots, \boldsymbol{r}_k|\boldsymbol{M}) \\ &\quad = \left[\frac{1}{\pi^N|\boldsymbol{M}|} e^{-\mathrm{tr}\{\boldsymbol{M}^{-1}\boldsymbol{T}_i\}}\right]^{K+1}, \ i = \{0, 1\} \end{aligned} \tag{13}$$

with

$$\boldsymbol{T}_0 = \frac{\boldsymbol{r}\boldsymbol{r}^{\dagger} + \sum_{k=1}^{K} \boldsymbol{r}_k\boldsymbol{r}_k^{\dagger}}{K+1} \tag{14}$$

and

$$\boldsymbol{T}_1 = \frac{(\boldsymbol{r} - \boldsymbol{H}(\Delta u, \Delta v)\boldsymbol{b})(\boldsymbol{r} - \boldsymbol{H}(\Delta u, \Delta v)\boldsymbol{b})^{\dagger} + \sum_{k=1}^{K} \boldsymbol{r}_k \boldsymbol{r}_k^{\dagger}}{K+1}. \tag{15}$$

The optimal Neyman-Pearson detector for the hypothesis testing problem (12), i.e., the LRT, cannot be implemented without the knowledge of Δu, Δv, $\boldsymbol{b}$, and $\boldsymbol{M}$. Moreover, another complication connected with the design of a practical detector relies on the fact that the number of unknowns in the array coupling coefficients, namely $P^2 - 1$, can be either assumed known or unknown. In this respect it is possible to explore GLRT-based detectors when the number of coupling coefficients is known at the design stage, while the case of unknown model order can be studied resorting to the MFLRT criterion.

A. Decision Statistic for Known P

In the following, the target detection problem (12) is addressed under the assumption of P known at the design stage. In this context, resorting to the GLRT criterion, the following decision rule can be defined

$$\frac{\max\limits_{\substack{\boldsymbol{M}\in\mathbb{H}_{++}^{MN},\boldsymbol{b}\in\mathbb{C}^{P^2} \\ \Delta u\in\mathcal{A},\Delta v\in\mathcal{B}}} f_{\mathcal{H}_1}(\boldsymbol{r}, \boldsymbol{r}_1, \ldots, \boldsymbol{r}_k | \boldsymbol{M}, \boldsymbol{b}, \Delta u, \Delta v)}{\max\limits_{\boldsymbol{M}\in\mathbb{H}_{++}^{MN}} f_{\mathcal{H}_0}(\boldsymbol{r}, \boldsymbol{r}_1, \ldots, \boldsymbol{r}_k | \boldsymbol{M})} \underset{\mathcal{H}_0}{\overset{\mathcal{H}_1}{\gtrless}} \gamma, \tag{16}$$

where γ is the detection threshold set to ensure a desired P_{fa}, $\mathcal{A}$ denotes the uncertainty set associated with Δu, i.e., $[-\alpha, \alpha]$, and $\mathcal{B}$ denotes the uncertainty set associated with Δv, i.e., $[-\beta, \beta]$. In this context, α and β are used to control the uncertainty region related to the unknown target DOA. It is important to emphasize that their values must be carefully chosen to guarantee a high level of accuracy of the array manifold approximation (10). To this end, a viable choice entails setting them to the 3dB single-side beamwidth $(u_{3dB}, v_{3dB}) \triangleq (0.891/N, 0.891/M)$ of a planar array when pointing in the boresight direction.[2]

Maximizing both the numerator and the denominator of (16) over $\boldsymbol{M}$ and taking their logarithm yields the decision statistic (after standard manipulation),

$$\begin{aligned} l_G &= 2(K+1)\log\left(\frac{|\boldsymbol{T}_0|}{\min\limits_{\boldsymbol{b},\ \Delta u\in\mathcal{A},\Delta v\in\mathcal{B}} |\boldsymbol{T}_1|}\right) \\ &= 2(K+1)\frac{1 + \boldsymbol{r}_w^{\dagger}\boldsymbol{r}_w}{1 + \min\limits_{\boldsymbol{b},\ \Delta u\in\mathcal{A},\Delta v\in\mathcal{B}} \|\boldsymbol{r}_w - \boldsymbol{H}_w(\Delta u, \Delta v)\boldsymbol{b}\|^2}, \end{aligned} \tag{17}$$

where $\boldsymbol{H}_w(\Delta u, \Delta v) = \boldsymbol{S}^{-1/2}\boldsymbol{H}(\Delta u, \Delta v) \in \mathbb{C}^{MN\times P^2}$ and $\boldsymbol{r}_w = \boldsymbol{S}^{-1/2}\boldsymbol{r} \in \mathbb{C}^{MN}$ are the quasi-whitened counterparts of $\boldsymbol{H}(\Delta u, \Delta v)$ and $\boldsymbol{r}$ respectively, with $\boldsymbol{S} = \sum_{k=1}^{K} \boldsymbol{r}_k \boldsymbol{r}_k^{\dagger} \in \mathbb{C}^{MN\times MN}$.

[2]Remarkably, a viable way to control the linearization-induced errors entails considering a partition of the 2D DOA uncertainty set in sub-intervals whereby bespoke linearization of the steering vector could be performed.

Hence, letting $\boldsymbol{\Delta\theta} = [\Delta u, \Delta v]^{\mathrm{T}} \in \mathbb{R}^2$, the optimization problem in (17) is equivalent to

$$\min_{\boldsymbol{b},\boldsymbol{\Delta\theta}\in\mathcal{S}} \|\boldsymbol{r}_w - \boldsymbol{H}_w(\boldsymbol{\Delta\theta})\boldsymbol{b}\|^2, \tag{18}$$

where $\mathcal{S} = [-\alpha, \alpha]\times[-\beta, \beta]$ denotes the nonempty and compact feasible set for $\boldsymbol{\Delta\theta}$. Let us now consider the optimization w.r.t. $\boldsymbol{b}$ in (18),

$$\hat{\boldsymbol{b}} = \arg\min_{\boldsymbol{b}} \|\boldsymbol{r}_w - \boldsymbol{H}_w(\boldsymbol{\Delta\theta})\boldsymbol{b}\|^2 = \boldsymbol{H}_w^o(\boldsymbol{\Delta\theta})\boldsymbol{r}_w, \tag{19}$$

where[3]

$$\boldsymbol{H}_w^o(\boldsymbol{\Delta\theta}) = \left(\boldsymbol{H}_w^{\dagger}(\boldsymbol{\Delta\theta})\boldsymbol{H}_w(\boldsymbol{\Delta\theta})\right)^{-1}\boldsymbol{H}_w^{\dagger}(\boldsymbol{\Delta\theta}) \tag{20}$$

is the Moore-Penrose inverse of $\boldsymbol{H}_w(\boldsymbol{\Delta\theta})$. Thus, by substituting the optimizer of $\boldsymbol{b}$ into (17) leads to

$$\tau_{\mathrm{GLRT-LAM}} = \frac{\max\limits_{\boldsymbol{\Delta\theta}\in\mathcal{S}} g(\boldsymbol{\Delta\theta})}{1 + \|\boldsymbol{r}_w\|^2}, \tag{21}$$

where $g(\boldsymbol{\Delta\theta}) = \boldsymbol{r}_w^{\dagger}\boldsymbol{P}_H(\boldsymbol{\Delta\theta})\boldsymbol{r}_w$ and $\boldsymbol{P}_H(\boldsymbol{\Delta\theta}) = \boldsymbol{H}_w(\boldsymbol{\Delta\theta})\boldsymbol{H}_w^o(\boldsymbol{\Delta\theta}) \in \mathbb{H}_{++}^{MN}$ is the projector onto the range span of $\boldsymbol{H}_w(\boldsymbol{\Delta\theta})$.

It remains to optimize (21) w.r.t. $\boldsymbol{\Delta\theta}$. To this end, let us recast the objective function in (21) as

$$\begin{aligned} g(\boldsymbol{\Delta\theta}) &= \boldsymbol{y}^{\dagger}\boldsymbol{A}^{-1}\boldsymbol{y}\Big|_{\substack{\boldsymbol{y}=\boldsymbol{H}_w^{\dagger}(\boldsymbol{\Delta\theta})\boldsymbol{r}_w \\ \boldsymbol{A}=\boldsymbol{H}_w^{\dagger}(\boldsymbol{\Delta\theta})\boldsymbol{H}_w(\boldsymbol{\Delta\theta})}} \\ &= \bar{g}(\boldsymbol{y}, \boldsymbol{A})\Big|_{\substack{\boldsymbol{y}=\boldsymbol{H}_w^{\dagger}(\boldsymbol{\Delta\theta})\boldsymbol{r}_w \\ \boldsymbol{A}=\boldsymbol{H}_w^{\dagger}(\boldsymbol{\Delta\theta})\boldsymbol{H}_w(\boldsymbol{\Delta\theta})}} \end{aligned} \tag{22}$$

where $\boldsymbol{y} \in \mathbb{C}^{P^2}$, $\boldsymbol{A} \in \mathbb{H}_{++}^{P^2}$, and $\bar{g}(\boldsymbol{y}, \boldsymbol{A})$ is jointly convex w.r.t. $\boldsymbol{A}$ and $\boldsymbol{y}$.

In order to tackle the challenging optimization problem at hand, an MM-based method [40], [41], [42], [43], [44], [45] is developed, which is an iterative procedure consisting of two distinct steps. The former involves the computation of an appropriate tight minorant (surrogate function) based on the current tentative solution. The latter entails its optimization, generating an updated estimate of the unknowns.

Following the same line of reasoning as in [13], the tangent plane $\bar{g}_a(\boldsymbol{y}, \boldsymbol{A}|\boldsymbol{y}_0, \boldsymbol{A}_0)$ to $\bar{g}(\boldsymbol{y}, \boldsymbol{A})$ in $(\boldsymbol{y}_0, \boldsymbol{A}_0)$ is an appropriate choice as surrogate function for the problem at hand. Precisely, it is defined as [13]

$$\begin{aligned} \bar{g}_a(\boldsymbol{y}, \boldsymbol{A}|\boldsymbol{y}_0, \boldsymbol{A}_0) &= \boldsymbol{y}_0^{\dagger}\boldsymbol{A}_0^{-1}\boldsymbol{y}_0 \\ &\quad + 2\,\mathrm{Re}\{\nabla_{\boldsymbol{y}}\bar{g}^{\dagger}(\boldsymbol{y}_0, \boldsymbol{A}_0)(\boldsymbol{y} - \boldsymbol{y}_0)\} \\ &\quad + \mathrm{tr}\{\nabla_{\boldsymbol{A}}\bar{g}(\boldsymbol{y}_0, \boldsymbol{A}_0)(\boldsymbol{A} - \boldsymbol{A}_0)\}, \end{aligned} \tag{23}$$

where

$$\nabla_{\boldsymbol{y}}\bar{g}(\boldsymbol{y}, \boldsymbol{A}) = \boldsymbol{A}^{-1}\boldsymbol{y} \tag{24}$$

and

$$\nabla_{\boldsymbol{A}}\bar{g}(\boldsymbol{y}, \boldsymbol{A}) = -\boldsymbol{A}^{-1}\boldsymbol{y}\boldsymbol{y}^{\dagger}\boldsymbol{A}^{-1} \tag{25}$$

[3]Notice that the assumption of $\boldsymbol{H}_1$ being full rank implies that, for any $\boldsymbol{\Delta\theta}$, $\boldsymbol{H}(\boldsymbol{\Delta\theta})$ is full rank as well. As an immediate proof, assuming by contradiction $\boldsymbol{H}(\boldsymbol{\Delta\theta})$ not full-rank, i.e., there exists a $\boldsymbol{\Delta\theta}$ for which at least one of its columns is a linear combination of the others, then one of the columns of $\boldsymbol{H}_1$ becomes a linear combination of the others, which contradicts the hypothesis of $\boldsymbol{H}_1$ being full rank.

are the gradients of $\bar{g}(\boldsymbol{y}, \boldsymbol{A})$ w.r.t. $\boldsymbol{A}$ and $\boldsymbol{y}$, respectively.

As a result, denoting by $\boldsymbol{\Delta\theta}^{\star(h-1)} = [\Delta u^{\star(h-1)}, \Delta v^{\star(h-1)}]^{\mathrm{T}}$ the output of the MM algorithm at the $(h-1)$−th iteration, it yields,

$$g(\boldsymbol{\Delta\theta}) \geq \bar{g}_a(\boldsymbol{y}, \boldsymbol{A}|\boldsymbol{y}_0^{(h-1)}, \boldsymbol{A}_0^{(h-1)})\Big|_{\substack{\boldsymbol{y}=\boldsymbol{H}_w^{\dagger}(\boldsymbol{\Delta\theta})\boldsymbol{r}_w \\ \boldsymbol{A}=\boldsymbol{H}_w^{\dagger}(\boldsymbol{\Delta\theta})\boldsymbol{H}_w(\boldsymbol{\Delta\theta})}} = g_a(\boldsymbol{\Delta\theta}|\boldsymbol{\Delta\theta}^{\star(h-1)}), \tag{26}$$

with $\boldsymbol{y}_0^{(h-1)} = \boldsymbol{H}_w^{\dagger}(\boldsymbol{\Delta\theta}^{\star(h-1)})\boldsymbol{r}_w$ and $\boldsymbol{A}_0^{(h-1)} = \boldsymbol{H}_w^{\dagger}(\boldsymbol{\Delta\theta}^{\star(h-1)})\boldsymbol{H}_w(\boldsymbol{\Delta\theta}^{\star(h-1)})$ while the equality in (26) holds when $\boldsymbol{\Delta\theta} = \boldsymbol{\Delta\theta}^{\star(h-1)}$. Then, exploiting the current estimated point $\boldsymbol{\Delta\theta}^{\star(h-1)}$, the optimization w.r.t. $\boldsymbol{\Delta\theta}$ at the h-th iteration can be obtained according to the maximization of the right-hand side (RHS) of (26), namely (after some algebra)

$$\boldsymbol{\Delta\theta}^{\star(h)} = \underset{\boldsymbol{\Delta\theta}\in\mathcal{S}}{\arg\max}\, g_a(\boldsymbol{\Delta\theta}|\boldsymbol{\Delta\theta}^{\star(h-1)}) \tag{27}$$

with $\boldsymbol{\Delta\theta}^{\star(h)}$ being the global (unique) optimum of the objective function at hand (the proof is reported in Appendix C). Moreover, the optimal solution to (27) is obtained according to the following proposition:

Proposition 1: The optimal solution $\boldsymbol{\Delta\theta}^{\star(h)}$ to (27) is given by the global optimal point for the unconstrained version of (27), i.e.,

$$\boldsymbol{\Delta\theta}^{\star(h)} = \Delta\boldsymbol{\theta}_1 = [\widetilde{\Delta u}, \widetilde{\Delta v}]^{\mathrm{T}}, \tag{28}$$

if this solution is feasible, i.e., $\Delta\boldsymbol{\theta}_1 \in \mathcal{S}$ with $\widetilde{\Delta u}$ and $\widetilde{\Delta v}$ given in Appendix D. Otherwise, the optimal solution is obtained by restricting the objective function to the boundaries of $\mathcal{S}$ and selecting the maximum among the finite set $\{\boldsymbol{\theta}_1, \ldots, \boldsymbol{\theta}_5\}$ of optimal candidate solutions, i.e.,

$$\boldsymbol{\Delta\theta}^{\star(h)} = \underset{\Delta\boldsymbol{\theta}\in\{\Delta\boldsymbol{\theta}_i\}_{i=2}^{5}}{\arg\max}\, g_a(\boldsymbol{\Delta\theta}|\boldsymbol{\Delta\theta}^{\star(h-1)}), \tag{29}$$

where

$$\begin{aligned} \Delta\boldsymbol{\theta}_2 &= [\Delta u_+^*, \beta]^{\mathrm{T}}, & \Delta\boldsymbol{\theta}_3 &= [\Delta u_-^*, -\beta]^{\mathrm{T}}, \\ \Delta\boldsymbol{\theta}_4 &= [\alpha, \Delta v_+^*]^{\mathrm{T}}, & \Delta\boldsymbol{\theta}_5 &= [-\alpha, \Delta v_-^*]^{\mathrm{T}}, \end{aligned} \tag{30}$$

with

$$\Delta u_{\pm}^* = \max(\min(-b'_{\pm\beta}/(2a'), \alpha), -\alpha), \tag{31}$$

$$\Delta v_{\pm}^* = \max(\min(-b''_{\pm\alpha}/(2a''), \beta), -\beta), \tag{32}$$

a', $b'_{\pm\beta}$, a'', and $b''_{\pm\alpha}$ are defined in Appendix D.

Proof: See Appendix D. ∎

A summary of the MM is reported in **Algorithm 1**, whereby the exit condition is assumed

$$|P^{(h)} - P^{(h-1)}| < \varepsilon_1, \tag{33}$$

where

$$P^{(h)} = g_a(\boldsymbol{\Delta\theta}^{\star(h)}|\boldsymbol{\Delta\theta}^{\star(h-1)}) \tag{34}$$

is the objective function at the h-th iteration and $\varepsilon_1 > 0$ is a user-defined exit threshold.

Algorithm 1 A Solution to (27) via MM

Input: $\boldsymbol{r}_w$, $\boldsymbol{H}_{0w} = \boldsymbol{S}^{-1/2}\boldsymbol{H}_0$, $\tilde{\boldsymbol{H}}_w$, $\hat{\boldsymbol{H}}_w$, $\bar{u}$, $\bar{v}$, α, β, ε_1.
Output: A solution $\widehat{\Delta\boldsymbol{\theta}}^{\star}$ to Problem (27) .

1. Set $h = 0$, $\Delta\boldsymbol{\theta}^{(h)} = [\Delta u^{(h)}, \Delta v^{(h)}]^{\mathrm{T}} = \boldsymbol{0}$, $P^{(h)} = \infty$.
2. **repeat**
3. $h = h + 1$;
4. Compute $\boldsymbol{H}_w(\boldsymbol{\Delta\theta}^{(h-1)}) = \boldsymbol{H}_{0w} + \tilde{\boldsymbol{H}}_w\Delta u^{(h-1)} + \hat{\boldsymbol{H}}_w\Delta v^{(h-1)}$;
5. Compute $\boldsymbol{y}_0^{(h-1)} = \boldsymbol{H}_w^{\dagger}(\boldsymbol{\Delta\theta}^{(h-1)})\boldsymbol{r}_w$ and $\boldsymbol{A}_0^{(h-1)} = \boldsymbol{H}_w^{\dagger}(\boldsymbol{\Delta\theta}^{(h-1)})\boldsymbol{H}_w(\boldsymbol{\Delta\theta}^{(h-1)})$;
6. Obtain $\Delta\boldsymbol{\theta}^{(h)}$ via Proposition 1;
8. Evaluate $P^{(h)} = g_a(\boldsymbol{\Delta\theta}^{(h)}|\boldsymbol{y}_0^{(h-1)}, \boldsymbol{A}_0^{(h-1)})$;
9. **until** $|P^{(h)} - P^{(h-1)}| < \varepsilon_1$.
10. Output $\widehat{\Delta\boldsymbol{\theta}}^{\star} = \Delta\boldsymbol{\theta}^{(h)} = [\widehat{\Delta u}^{\star}, \widehat{\Delta v}^{\star}]^{\mathrm{T}}$.

Therefore, exploiting the result of **Algorithm 1**, the GLRT for Linearized Array Manifold (GLRT-LAM) statistic is defined by

$$\tau_{\mathrm{GLRT-LAM}} = \frac{\boldsymbol{r}_w^{\dagger}\boldsymbol{P}_H\left(\widehat{\Delta u}^{\star}, \widehat{\Delta v}^{\star}\right)\boldsymbol{r}_w}{1 + \|\boldsymbol{r}_w\|^2}. \tag{35}$$

Furthermore, as long as the number of iterations involved in the MM procedures is limited, the computational complexity is dominated by the evaluation of the sample covariance matrix $\boldsymbol{S}$, that is $\mathcal{O}(MNK)$. As a final remark, following the same approach as in [13] for the case of ULA, it is straightforward to prove that the derived GLRT-LAM detection architecture verifies the bounded-constant false alarm rate (CFAR) property.

B. Decision Statistic for Unknown P

In this subsection, the target detection problem is addressed for the case where the actual number of MC coefficients is unknown. This entails an additional complexity in the development of a tailored processing scheme for target information extraction. To deal with this problem, a multiple composite alternative hypothesis testing problem is formulated, with each alternative hypothesis pertaining to a given number of unknown signal parameters. Formally,

$$\begin{cases} \mathcal{H}_0 : \begin{cases} \boldsymbol{r} = \boldsymbol{n} \\ \boldsymbol{r}_k = \boldsymbol{n}_k, \quad k = 1, \ldots, K \end{cases} \\ \mathcal{H}_i : \begin{cases} \boldsymbol{r} = \boldsymbol{H}_i(\Delta u, \Delta v)\boldsymbol{b}_i + \boldsymbol{n} \\ \boldsymbol{r}_k = \boldsymbol{n}_k, \quad k = 1, \ldots, K \end{cases}, \quad i = 1, \ldots, \bar{N}, \end{cases} \tag{36}$$

where $\bar{N} \leq MN/2$ is the maximum[4] allowed model order,

$$\boldsymbol{H}_i(\Delta u, \Delta v) = \boldsymbol{H}_{0i} + \tilde{\boldsymbol{H}}_i\Delta u + \hat{\boldsymbol{H}}_i\Delta v, \tag{37}$$

and

$$\boldsymbol{b}_i = [\bar{\boldsymbol{b}}_1^{\mathrm{T}}, \bar{\boldsymbol{b}}_2^{\mathrm{T}}, \ldots, \bar{\boldsymbol{b}}_i^{\mathrm{T}}]^{\mathrm{T}}, \tag{38}$$

with

[4]An appropriate upper-bound $\bar{N}$ to the maximum model order can be reasonably considered, supported by physical or empirical considerations. It is also worth noting that $\bar{N} \leq MN/2$ ensures model identifiability.

- $\boldsymbol{H}_{0i} = \left[\boldsymbol{D}_0\boldsymbol{p}_u \otimes \boldsymbol{J}_v, \boldsymbol{D}_1\boldsymbol{p}_u \otimes \boldsymbol{J}_v, \ldots, \boldsymbol{D}_{i-1}\boldsymbol{p}_u \otimes \boldsymbol{J}_v\right]$;
- $\tilde{\boldsymbol{H}}_i = \left[\boldsymbol{D}_0\dot{\boldsymbol{p}}_u \otimes \boldsymbol{J}_v, \boldsymbol{D}_1\dot{\boldsymbol{p}}_u \otimes \boldsymbol{J}_v, \ldots, \boldsymbol{D}_{i-1}\dot{\boldsymbol{p}}_u \otimes \boldsymbol{J}_v\right]$;
- $\hat{\boldsymbol{H}}_i = \left[\boldsymbol{D}_0\boldsymbol{p}_u \otimes \dot{\boldsymbol{J}}_v, \boldsymbol{D}_1\boldsymbol{p}_u \otimes \dot{\boldsymbol{J}}_v, \ldots, \boldsymbol{D}_{i-1}\boldsymbol{p}_u \otimes \dot{\boldsymbol{J}}_v\right]$.

Remarkably, since the alternative hypotheses are nested in (36), i.e., $\mathcal{H}_i \subset \mathcal{H}_j,\ i < j$, a viable solution to handle (36) is to resort to the MFLRT framework [32]. Thus, the target presence can be established according to the decision rule

$$\tau_{\text{MFLRT}} = \max_{1\le i\le \bar{N}}\left\{\left[l_G^{(i)} - 2(i^2+1)\left(\log\left(\frac{l_G^{(i)}}{2(i^2+1)}\right)+1\right)\right] u\left(\frac{l_G^{(i)}}{2(i^2+1)} - 1\right)\right\} > \bar{\gamma}, \tag{39}$$

where

- $2(i^2+1)$ is the number of unknown parameters under the $\mathcal{H}_i$ hypothesis;[5]
- $l_G^{(i)}$ is the GLRT-like statistic (17) derived assuming $P = i$;
- $\bar{\gamma}$ is the threshold guaranteeing the demanded P_{fa};
- $u(t)$ is the unit step function, i.e., $u(t) = 1$ as long as $t \ge 0$ and zero otherwise.

Specifically, denoting by $\widehat{\boldsymbol{\Delta\theta}}_{\text{MM}}^{(i)}$ the estimate of the directional cosines displacements provided by **Algorithm 1** assuming $P = i$,

$$l_G^{(i)} = 2(K+1)\frac{1 + \boldsymbol{r}_w^\dagger\boldsymbol{r}_w}{1 + \|\boldsymbol{r}_w\|^2 - \boldsymbol{r}_w^\dagger\boldsymbol{P}_H\left(\widehat{\boldsymbol{\Delta\theta}}_{\text{MM}}^{(i)}\right)\boldsymbol{r}_w}. \tag{40}$$

Finally, by following the same methodology used in [13] for ULA, it can be easily proven that the derived MLRT-LAM detector (39) also satisfies the bounded-CFAR property.

IV. Simulation Results

In this section, numerical examples are provided to evaluate both the detection and estimation capabilities of the proposed processing schemes for a URA with $M = 5$ and $N = 6$ in the presence of MC. The inter-element spacing among the antennas is set to half wavelength and the number of secondary data is $K = 4MN = 120$. Moreover, the uncertainty set where the unknown target DOA is assumed lying is defined by $\alpha = u_{3dB} \triangleq 0.891/M = 0.1782$ and $\beta = v_{3dB} \triangleq 0.891/N = 0.1485$, where u_{3dB} and v_{3dB} are the 3 dB single-side beamwidth of a planar array pointing at the boresight direction. It is also assumed that the pointing direction is $(\theta, \phi) = (33°, 73°)$. As to the target location parameters, two cases are analyzed. The former considers cosine mismatches $[\Delta u, \Delta v]^{\text{T}} = [0, 0]^{\text{T}}$, whereas the latter assumes $[\Delta u, \Delta v]^{\text{T}} = [0.03, 0.05]^{\text{T}}$. Consequently, the robustness of the developed methods to MC is mainly evaluated through the former analysis, whereas the latter highlights their capabilities to handle mismatches induced by both MC and DOA displacement jointly. Furthermore, to model the MC between the array elements, the following values of the coupling coefficients are supposed in the simulations, assuming $P = 3$:

- $\boldsymbol{c}_1 = [1, 0.75 + 0.48j, 0.67 + 0.32j]^{\text{T}}$,
- $\boldsymbol{c}_2 = [0.58 + 0.29j, 0.42 - 0.35j, 0.39 + 0.24j]^{\text{T}}$,
- $\boldsymbol{c}_3 = [0.03 + 0.45j, 0.12 - 0.31j, 0.09 - 0.18j]^{\text{T}}$.

Moreover, in order to assess the detection performance, the P_d is used as evaluation criterion, computed resorting to $N_{MC} = 5000$ Monte Carlo runs and assuming a Probability of False Alarm (P_{fa}) equals to 10^{-4}. In this respect, $\frac{100}{P_{fa}}$ Monte Carlo trails are evaluated to set the detection thresholds of the considered detectors. As to the estimation performance, needless to say evaluated under $\mathcal{H}_1$, the RMSE is considered as figure of merit. It is computed as

$$\text{RMSE}_{\Delta u} = \sqrt{\frac{1}{N_{MC}}\sum_{r=1}^{N_{MC}}\left|\Delta u - \widehat{\Delta u}_r\right|^2},$$

and

$$\text{RMSE}_{\Delta v} = \sqrt{\frac{1}{N_{MC}}\sum_{r=1}^{N_{MC}}\left|\Delta v - \widehat{\Delta v}_r\right|^2},$$

where $\widehat{\Delta u}_r$ and $\widehat{\Delta v}_r$ are the estimates provided at the r-th trial by a given technique.

Furthermore, the SINR is defined as

$$\text{SINR} = |a|^2\boldsymbol{p}_m^\dagger(u_0, v_0)\boldsymbol{M}^{-1}\boldsymbol{p}_m(u_0, v_0). \tag{41}$$

For the evaluation of the MFLRT-based methods, $\bar{N} \in \{2, 3, 4\}$ is analyzed, where the value of $\bar{N}$ is specified as subscript. Furthermore, the two-stage (referred to as "2S") architectures of both the derived GLRT-based and MFLRT-based methods is also implemented, namely, after a first computation of the unknown angular displacement $\widehat{\Delta\boldsymbol{\theta}}^\star = [\widehat{\Delta u}^\star, \widehat{\Delta v}^\star]^{\text{T}}$ (as described in Section III), the ideal steering vector (8) is re-linearized around $(\bar{u} + \widehat{\Delta u}^\star, \bar{v} + \widehat{\Delta v}^\star)$ and the estimation procedure is executed once again.

For comparison, the following detectors are also included:

- the GLRT using the actual array manifold with known target DOA and known coupling coefficients

$$\tau_{\text{GLRT-ben}} = \frac{|\boldsymbol{p}_m^\dagger(u_0, v_0)\boldsymbol{S}^{-1}\boldsymbol{r}|^2}{(1 + \boldsymbol{r}^\dagger\boldsymbol{S}^{-1}\boldsymbol{r})\boldsymbol{p}_m^\dagger(u_0, v_0)\boldsymbol{S}^{-1}\boldsymbol{p}_m(u_0, v_0)}; \tag{42}$$

- the GLRT using the ideal array manifold (not encompassing the MC phenomenon) with known target DOA

$$\tau_{\text{GLRT-ben-NC}} = \frac{|\boldsymbol{p}^\dagger(u_0, v_0)\boldsymbol{S}^{-1}\boldsymbol{r}|^2}{(1 + \boldsymbol{r}^\dagger\boldsymbol{S}^{-1}\boldsymbol{r})\boldsymbol{p}^\dagger(u_0, v_0)\boldsymbol{S}^{-1}\boldsymbol{p}(u_0, v_0)}; \tag{43}$$

- the GLRT using the actual array manifold with known target DOA but with the useful target steering vector affected by the MC phenomenon

$$\tau_{\text{GLRT-ben-DOA}} = \frac{\boldsymbol{r}_w^\dagger\boldsymbol{P}_{\boldsymbol{H}_{t,w}}\boldsymbol{r}_w}{1 + \|\boldsymbol{r}_w\|^2}, \tag{44}$$

where $\boldsymbol{P}_{\boldsymbol{H}_{t,w}} = \boldsymbol{H}_{t,w}\left(\boldsymbol{H}_{t,w}^\dagger\boldsymbol{H}_{t,w}\right)^{-1}\boldsymbol{H}_{t,w}^\dagger$ with $\boldsymbol{H}_{t,w} = \boldsymbol{S}^{-1/2}\left[\boldsymbol{D}_0\boldsymbol{p}_u(u_0) \otimes \boldsymbol{J}_{v_0}, \ldots, \boldsymbol{D}_{P-1}\boldsymbol{p}_u(u_0) \otimes \boldsymbol{J}_{v_0}\right]$ and $\boldsymbol{J}_{v_0} = [\boldsymbol{p}_v(v_0), \boldsymbol{J}_1\boldsymbol{p}_v(v_0), \ldots, \boldsymbol{J}_{P-1}\boldsymbol{p}_v(v_0)]$;

- the standard GLRT using the ideal array manifold with the nominal pointing direction $(\bar{u}, \bar{v})$ (which refers to a

[5]Under the $\mathcal{H}_i$ hypothesis, the total number of unknowns are given by the two DOA displacements Δu and Δv, and the i^2 complex MC coefficients.

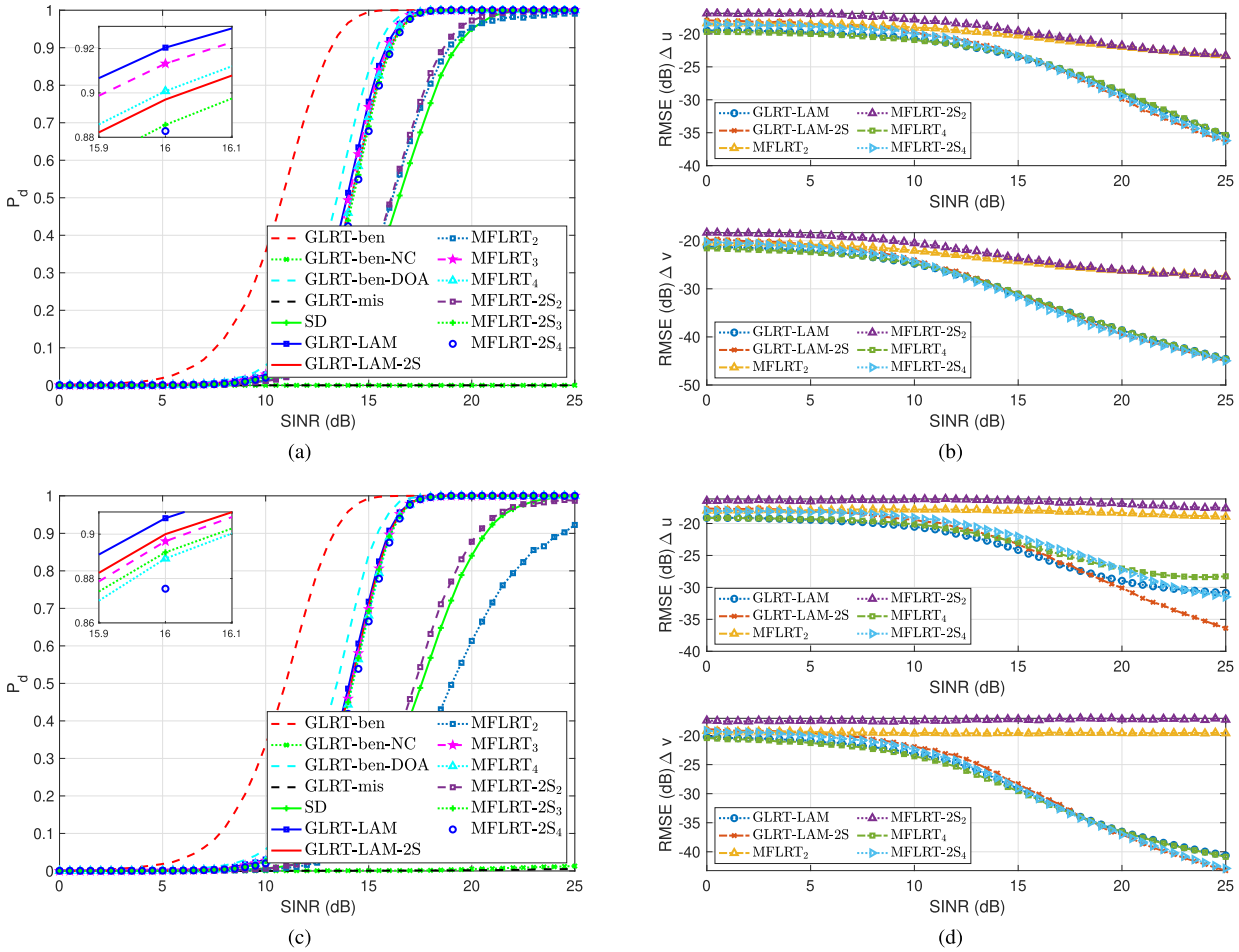

Fig. 4. P_d (left figures) and RMSE (right figures) versus SINR in the background of Gaussian white noise, assuming (a) and (b) $[\Delta u, \Delta v]^{\mathrm{T}} = [0, 0]^{\mathrm{T}}$; (c) and (d) $[\Delta u, \Delta v]^{\mathrm{T}} = [0.03, 0.05]^{\mathrm{T}}$.

fully mismatched case) [20]

$$\tau_{\text{GLRT-mis}} = \frac{|\boldsymbol{p}^{\dagger}(\bar{u}, \bar{v})\boldsymbol{S}^{-1}\boldsymbol{r}|^2}{(1 + \boldsymbol{r}^{\dagger}\boldsymbol{S}^{-1}\boldsymbol{r})\boldsymbol{p}^{\dagger}(\bar{u}, \bar{v})\boldsymbol{S}^{-1}\boldsymbol{p}}; \tag{45}$$

- the Subspace Detector (SD) [46], namely a mismatched GLRT detector using as useful signal directions those given by the columns of $\boldsymbol{H}_{SD}$, i.e.,

$$\tau_{\text{SD}} = \frac{\boldsymbol{r}^{\dagger}\boldsymbol{S}^{-1}\boldsymbol{H}_{SD}\left(\boldsymbol{H}_{SD}^{\dagger}\boldsymbol{S}^{-1}\boldsymbol{H}_{SD}\right)^{-1}\boldsymbol{H}_{SD}^{\dagger}\boldsymbol{S}^{-1}\boldsymbol{r}}{1 + \boldsymbol{r}^{\dagger}\boldsymbol{S}^{-1}\boldsymbol{r}}, \tag{46}$$

with $\boldsymbol{H}_{SD} = [\boldsymbol{p}, \hat{\boldsymbol{p}}_u, \hat{\boldsymbol{p}}_v]$.

In the reported simulations, three different scenarios are examined. First, the useful signal is assumed buried in white Gaussian noise; then, a jamming interference situation is assessed. Finally, within this last context, random perturbations in the elements of the MCM are considered.

A. Gaussian White Noise Case

In this case study, the disturbance covariance matrix is modeled as $\boldsymbol{M} = \sigma_n^2\boldsymbol{I}_{MN}$ with σ_n^2 the internal noise power level, which is assumed, without loss of generality, equal to 0 dB.

The P_d curves versus SINR obtained in the aforementioned scenario for $[\Delta u, \Delta v]^{\mathrm{T}} = [0, 0]^{\mathrm{T}}$ and $[\Delta u, \Delta v]^{\mathrm{T}} = [0.03, 0.05]^{\mathrm{T}}$ are plotted in Figs. 4(a) and 4(c), respectively, with the corresponding RMSE versus SINR curves displayed in Figs. 4(b) and 4(d). Not surprisingly, the P_d results pertaining to the first analyzed DOAs scenario, depicted in Fig. 4 (a), reveal that the GLRT-ben and the GLRT-ben-DOA yield upper bounds to the performance of all the considered detectors. As to the devised strategies, both the GLRT-LAM and the MFLRT (but for the case $\bar{N} = 2$, where an undersized model order is considered), are able to provide satisfactory detection results, yielding performance close to that of the GLRT-ben-DOA. Specifically, the gap between the corresponding curves is less than 1 dB at $P_d = 0.9$. As already slightly pinpointed, inspection of the figure highlights that using $\bar{N} = 2$ for the computation of the MFLRT entails an inadequate signal model that leads to a SINR loss, at $P_d = 0.9$, in the order of 3 dB w.r.t. the GLRT-LAM. Furthermore, the second stage of processing is unable to provide any improvement in the detection performance, with a negligible loss w.r.t. the corresponding one stage curves. This is not surprising, as the best expansion point has already been used in the first linearization. Finally, the performance of the detectors that do not account for the coupling phenomenon, i.e., ben-GLRT-NC and GLRT-mis,

is unsatisfactory, with the only exception of the SD, which is instead capable to deliver acceptable performance, although inferior compared to the proposed strategies. This behavior reinforces the need for the development of tailored signal processing schemes to cope with the challenges posed by the MC. The capabilities of the devised strategies are also corroborated by the analysis of the estimation performance reported in Fig. 4 (b), within the Δu and Δv domains, respectively. In particular, looking over the plots highlights that both the GLRT and MFLRT methods (with the exception of the MFLRT_2) yield reliable estimates of the DOA displacements. Moreover, the 2S variants of the GLRT and MFLRT architectures deliver almost the same estimation performance, with slight improvement only in the high SINR regime.

Regarding the other DOAs scenario, i.e., $[\Delta u, \Delta v]^{\mathrm{T}} = [0.03, 0.05]^{\mathrm{T}}$, illustrated in Figs. 4 (c) and (d), the detection performance of the devised methods remains relatively unchanged as compared to the previously analyzed case, indicating that they are able to severely handle the mismatch caused by DOA uncertainty and to endow robustness to the joint detection and estimation process in the presence of MC effects. Furthermore, both the MFLRT_2 (and its 2S variant) and the SD scheme experience a performance loss, compared to the case presented in Fig. 4 (a), of approximately 1 dB at $P_d = 0.9$, reasonably due to the stronger mismatch on the signal model. The highlighted behavior of the devised methods is also pinpointed by the inspection of the RMSE curves, depicted in Fig. 4 (d). At low and medium SINR regimes, the achieved estimation performance is quite similar to that analyzed in the previous DOAs scenario, with some significant differences especially at high SINR. In particular, the estimates of Δu obtained with the 1S version of the proposed methods saturate, while those obtained with the 2S variants perform considerably better. In fact, the GLRT-LAM-2S provides increasingly accurate estimation performance as the SINR increases. This improvement is difficult to observe in the P_d curves since it is attained for SINR values where the detection performance of the aforementioned methods has substantially already achieved saturation.

B. Interference Case

In this section, the radar system is assumed affected by some interference from two narrowband jammers, angularly located at $(u_1, v_1) = (0.4698, 0.1710)$ and $(u_2, v_2) = (0.5567, 0.6634)$, respectively. As a consequence, the interference-plus-noise covariance matrix can be modeled as [47]

$$\boldsymbol{M} = \sum_{i=1}^{2} \sigma_i^2 \boldsymbol{p}_m(u_i, v_i) \boldsymbol{p}_m^{\dagger}(u_i, v_i) + \sigma_n^2 \boldsymbol{I}_{MN}, \tag{47}$$

where $\boldsymbol{p}_m(u_i, v_i)$ denotes the actual steering vector of the i-th ($i = 1, 2$) interference source with σ_1^2 and σ_2^2 the corresponding powers. Moreover, it is assumed that the Jammer to Noise Ratio (JNR) of the two emitters is $JNR_1 \triangleq \sigma_1^2/\sigma_n^2 = 30$ dB and $JNR_2 \triangleq \sigma_2^2/\sigma_n^2 = 40$ dB, respectively.

The effectiveness of the methods under consideration are analyzed in Fig. 5, using the same simulation setup considered in Fig. 4 but for the interference scenario which is now modeled according to (47). Specifically, the P_d curves evaluated assuming $[\Delta u, \Delta v]^{\mathrm{T}} = [0, 0]^{\mathrm{T}}$ are displayed in Fig. 5 (a), which shows no significant differences as compared to the corresponding white noise case. As a result, all detectors maintain their rankings. Still, a clear performance advantage over the mismatched and SD detectors is present, corroborating the effectiveness of the proposed strategies. Furthermore, the estimation performance, depicted in Fig. 5 (b), is consistent with the white noise disturbance situation as well, with only a slight loss (experienced by all the methods) on the inference of Δu, especially at the high SINR regime.

On the other hand, regarding the P_d behavior for $[\Delta u, \Delta v]^{\mathrm{T}} = [0.03, 0.05]^{\mathrm{T}}$ DOAs case, displayed in Fig. 5 (c), it is possible to observe detection performance similar to the case related to Fig. 4 (c), although with a slight improvement obtained by the 2S variants over the corresponding 1S counterparts. As a matter of fact, the RMSE curves in Fig. 5 (d) indicate a corresponding interesting performance improvement at high values of SINR. Specifically, starting from 22 dB in the Δu domain and 15 dB in the Δv domain, some advantages of our refined 2S processing scheme can be observed. Notably, being at this SINR regime the P_d not yet achieved saturation, detection gains are experienced too. Remarkably, the 2S strategy exploits the DOA estimation obtained in the first stage and provides, with the second stage, a more accurate approximation of the actual array manifold, resulting in improved performance and yielding accurate DOA estimates without saturation.

C. Perturbations in the Actual MCM

In practice, some perturbations on the nominal banded symmetric Toeplitz block Toeplitz structure of the MCM could be experienced, as for instance induced by radome reflection effects, sensor position misplacements, as well as changes in the environment (e.g., due to the movement of metal objects near the antenna array) [2] that might induce deviations in the nominal conditions of the radar system. To this end, possible random perturbation can be accounted for via the MCM model[6]

$$\hat{\boldsymbol{C}} = \boldsymbol{C} + \boldsymbol{N}_{pert}, \tag{48}$$

where $\boldsymbol{N}_{pert} \in \mathbb{C}^{N \times N} \sim \mathcal{CN}(0, \xi \boldsymbol{I})$ is a random perturbation matrix whose complex entries are modeled as independent and identically distributed zero-mean circularly-symmetric complex Gaussian random variables, with variance $\xi \geq 0$.

Within the same setup of Figs. 5 (c) and (d) correspondingly, in particular, to $[\Delta u, \Delta v]^{\mathrm{T}} = [0.03, 0.05]^{\mathrm{T}}$, the aim of the subsequent analysis is a robustness analysis of the devised GLRT- and MFLRT-based signal processing strategies considering, at each Monte Carlo trial, a different realization of the random perturbation term $\boldsymbol{N}_{pert}$, assuming $\xi = 0.1$. The results, presented in terms of P_d and RMSE versus SINR, are shown in Fig. 6. A comparison of the detection and estimation results with those obtained in the absence of perturbations,

[6]To keep the physical meaning of the MCM, the diagonal elements of $\hat{\boldsymbol{C}}$ are set to 1.

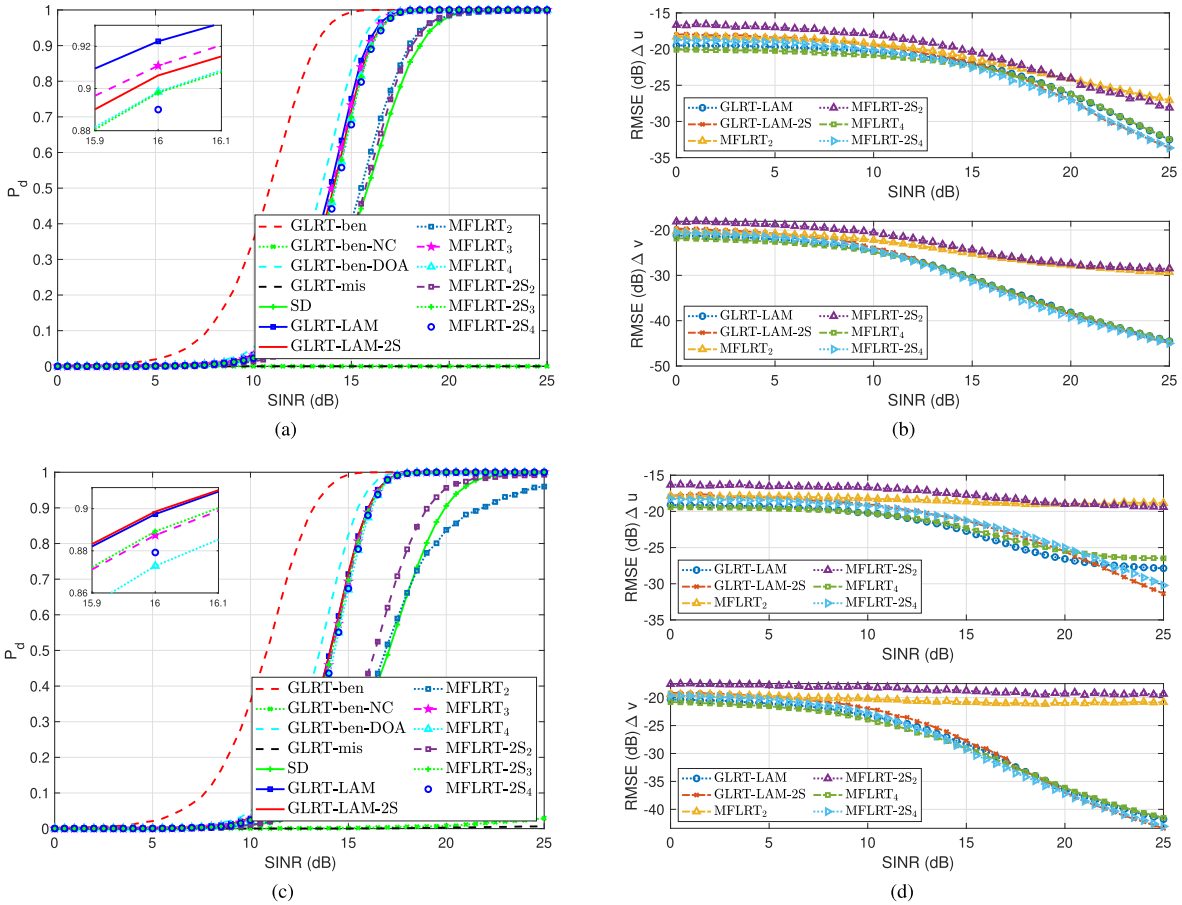

Fig. 5. P_d (left figures) and RMSE (right figures) versus SINR in an interference background, assuming (a) and (b) $[\Delta u, \Delta v]^{\mathrm{T}} = [0, 0]^{\mathrm{T}}$; (c) and (d) $[\Delta u, \Delta v]^{\mathrm{T}} = [0.03, 0.05]^{\mathrm{T}}$.

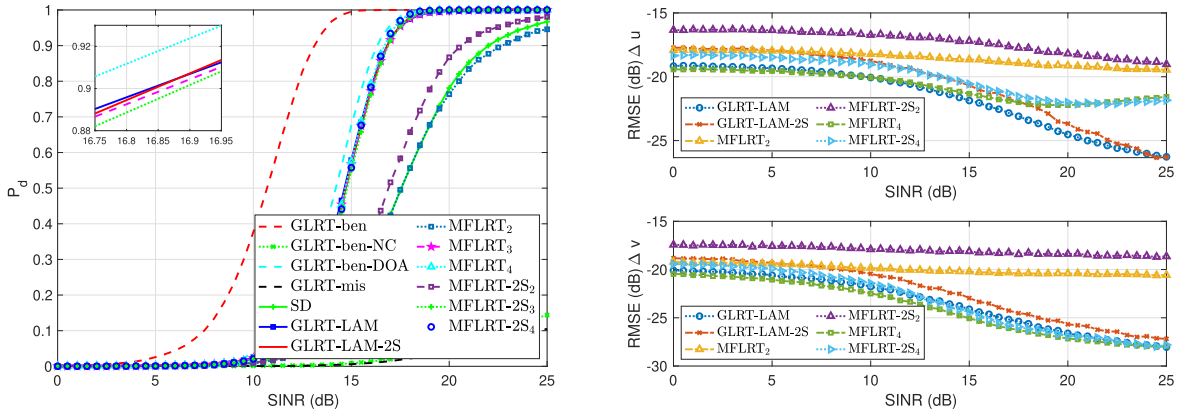

Fig. 6. P_d (left figures) and RMSE (right figures) versus SINR in an interference background and perturbations in the actual MCM, assuming $[\Delta u, \Delta v]^{\mathrm{T}} = [0.03, 0.05]^{\mathrm{T}}$.

analyzed in Figs. 5 (c) and (d), shows that the perturbations induce a detection performance degradation of approximately 1 dB at $P_d = 0.9$ for all considered methods. Moreover, unlike the corresponding ideal case, the MFLRT$_4$ and its 2S variant exhibit detection capabilities quite close to the ben-GLRT-DOA, with a slight advantage over the GLRT-LAM and GLRT-LAM-2S counterparts. This is attributed to the MFLRT capability to leverage higher model orders, which induces more degrees of freedom for the subsumed array manifold inference, thereby counteracting the effects of perturbations in the structure. This behavior is also reflected in the RMSE curves depicted in Fig. 6 (b). Specifically, at a low SINR regime, the MFLRT$_4$ yields the best performance in both Δu and Δv domains while at high SINR values, it achieves the best performance only for the Δv estimation, showing a performance saturation in the estimation of Δu. Still, in the high SINR regime, only the GLRT-LAM and its 2S variant do not experience a performance saturation in both the Δu and Δv domains, likely due to their prior knowledge of the number of active MC coefficients. Summarizing, the proposed techniques exhibit a good level of robustness to perturbations in the banded symmetric Toeplitz block Toeplitz structure of

the MCM, providing performance levels that are comparable to the nominal case, assumed at the design stage, where the MCM is modeled according to (5).

V. Conclusion

Simultaneous target detection and 2D DOA estimation for a URA affected by MC has been addressed. At the modeling stage, a suitable description of the actual echo return has been developed accounting for the unknown target 2D angular displacements w.r.t. the pointing direction and an unknown structured matrix that embeds the effects of MC and target backscattering. Leveraging this bespoke model, the target detection problem in Gaussian interference has been formulated and tackled by resorting to two sub-optimal criteria, i.e., the GLRT and the MFLRT. The former is adopted for the known model order case whereas the latter considers the situation where the number of actual coupling coefficients is unknown. The practical implementation of the detectors has demanded the joint ML estimates of the unknown angular displacements and coupling coefficients which stem as the solution to a non-convex optimization problem. To get a good quality solution, an *ad-hoc* iterative procedure based on the MM algorithm has been designed. It involves at each iteration the solution of a box-constrained quadratic optimization problem whose optimal point has been obtained in a closed form. Remarkably, both the GLRT and the MFLRT ensure the bounded-CFAR property. At the analysis stage, the performance of the proposed signal processing strategies has been assessed in terms of P_d and DOA RMSE in different scenarios, including the presence of jammers as well as random perturbations in the coupling matrix structure assumed at the design stage. Comparisons with benchmark detectors and some counterparts that do not encompass the MC phenomenon have also been conducted. The results have highlighted the effectiveness of the devised architectures showing performance levels comparable to the benchmark that assume known target DOA and model order.

Possible future research avenues might include the analysis on real (or on high-fidelity electromagnetically simulated) phased array data to assess possible discrepancies with the theoretical results, the derivation of additional decision statistics based on different criteria, such as Adaptive Matched Filter (AMF) [48], Rao, and Wald tests [31], as well as the application of the devised framework in a pulse-Doppler scenario accounting, at the design stage, for both the Doppler uncertainty and the MC effect. Finally, the extension to the multi-polarization case [49] could be definitely an interesting complement to this work.

Appendix

A. First Order Derivatives of the URA Spatial Steering Vector

According to (1), the derivatives of $\boldsymbol{p}$ w.r.t. u and v, evaluated respectively at $\bar{u}$ and $\bar{v}$, can be calculated as

$$\begin{aligned}\dot{\hat{\boldsymbol{p}}}_u &= \left.\frac{\partial \boldsymbol{p}(u,v)}{\partial u}\right|_{u=\bar{u}} = \left.\frac{\partial \boldsymbol{p}_u}{\partial u}\right|_{u=\bar{u}} \otimes \boldsymbol{p}_v(\bar{v}) \\ &= j2\pi\frac{d}{\lambda_0}\boldsymbol{E}_u\boldsymbol{p}_u(\bar{u}) \otimes \boldsymbol{p}_v(\bar{v}) \\ &= \dot{\boldsymbol{p}}_u \otimes \boldsymbol{p}_v(\bar{v}), \end{aligned} \tag{49}$$

and

$$\begin{aligned}\dot{\hat{\boldsymbol{p}}}_v &= \left.\frac{\partial \boldsymbol{p}(u,v)}{\partial v}\right|_{v=\bar{v}} = \boldsymbol{p}_u(\bar{u}) \otimes \left.\frac{\partial \boldsymbol{p}_v}{\partial v}\right|_{v=\bar{v}} \\ &= \boldsymbol{p}_u(\bar{u}) \otimes j2\pi\frac{d}{\lambda_0}\boldsymbol{E}_v\boldsymbol{p}_v(\bar{v}) \\ &= \boldsymbol{p}_u(\bar{u}) \otimes \dot{\boldsymbol{p}}_v, \end{aligned} \tag{50}$$

with $\dot{\boldsymbol{p}}_u = j2\pi\frac{d}{\lambda_0}\boldsymbol{E}_u\boldsymbol{p}_u(\bar{u})$, $\dot{\boldsymbol{p}}_v = j2\pi\frac{d}{\lambda_0}\boldsymbol{E}_v\boldsymbol{p}_v(\bar{v})$, $\boldsymbol{E}_u = \mathrm{diag}\big([0,1,\ldots,M-1]^{\mathrm{T}}\big) \in \mathbb{C}^{M\times M}$ and $\boldsymbol{E}_v = \mathrm{diag}\big([0,1,\ldots,N-1]^{\mathrm{T}}\big) \in \mathbb{C}^{N\times N}$.

B. Derivations of (11)

Expression (11) can be recast as

$$\begin{aligned} a\boldsymbol{p}_{am}(\Delta u,\Delta v) &= \boldsymbol{B}\boldsymbol{p}_a(\Delta u,\Delta v) \\ &= \boldsymbol{B}\boldsymbol{p} + \boldsymbol{B}\dot{\hat{\boldsymbol{p}}}_u\Delta u + \boldsymbol{B}\dot{\hat{\boldsymbol{p}}}_v\Delta v. \end{aligned} \tag{51}$$

The first term in (51) can be written as

$$\begin{aligned}\boldsymbol{B}\boldsymbol{p} &= \left(\sum_{i=0}^{P-1}\boldsymbol{D}_i \otimes a\boldsymbol{C}_{i+1}\right)\big(\boldsymbol{p}_u \otimes \boldsymbol{p}_v\big) \\ &= \sum_{i=0}^{P-1}\boldsymbol{D}_i\boldsymbol{p}_u \otimes a\boldsymbol{C}_{i+1}\boldsymbol{p}_v = \sum_{i=0}^{P-1}\boldsymbol{D}_i\boldsymbol{p}_u \otimes \boldsymbol{J}_v\bar{\boldsymbol{b}}_{i+1} \\ &= \sum_{i=0}^{P-1}(\boldsymbol{D}_i\boldsymbol{p}_u \otimes \boldsymbol{J}_v)\bar{\boldsymbol{b}}_{i+1} = \boldsymbol{H}_0\boldsymbol{b}, \end{aligned} \tag{52}$$

where

- $\boldsymbol{H}_0 = \big[\boldsymbol{D}_0\boldsymbol{p}_u \otimes \boldsymbol{J}_v, \boldsymbol{D}_1\boldsymbol{p}_u \otimes \boldsymbol{J}_v, \ldots, \boldsymbol{D}_{P-1}\boldsymbol{p}_u \otimes \boldsymbol{J}_v\big] \in \mathbb{C}^{MN\times P^2}$;
- $\boldsymbol{J}_v = [\boldsymbol{p}_v, \boldsymbol{J}_1\boldsymbol{p}_v, \ldots, \boldsymbol{J}_{P-1}\boldsymbol{p}_v] \in \mathbb{C}^{N\times P}$;
- $\boldsymbol{b} = [\bar{\boldsymbol{b}}_1^{\mathrm{T}}, \bar{\boldsymbol{b}}_2^{\mathrm{T}}, \ldots, \bar{\boldsymbol{b}}_P^{\mathrm{T}}]^{\mathrm{T}} \in \mathbb{C}^{P^2}$ with $\bar{\boldsymbol{b}}_l = [ac_{l,0}, ac_{l,1}, \ldots, ac_{l,P-1}]^{\mathrm{T}} \in \mathbb{C}^P$, $l = 1,\ldots,P$.

Similarly, the second term in (51) can be expressed as

$$\begin{aligned}\boldsymbol{B}\dot{\hat{\boldsymbol{p}}}_u\Delta u &= \left(\sum_{0=1}^{P-1}\boldsymbol{D}_i \otimes a\boldsymbol{C}_{i+1}\right)\big(\dot{\boldsymbol{p}}_u \otimes \boldsymbol{p}_v\big)\Delta u \\ &= \left(\sum_{i=0}^{P-1}(\boldsymbol{D}_i \otimes \boldsymbol{J}_v)(\dot{\boldsymbol{p}}_u \otimes \bar{\boldsymbol{b}}_{i+1})\right)\Delta u \\ &= \tilde{\boldsymbol{H}}\boldsymbol{b}\Delta u, \end{aligned} \tag{53}$$

where $\tilde{\boldsymbol{H}} = \big[\boldsymbol{D}_0\dot{\boldsymbol{p}}_u \otimes \boldsymbol{J}_v, \boldsymbol{D}_1\dot{\boldsymbol{p}}_u \otimes \boldsymbol{J}_v, \ldots, \boldsymbol{D}_{P-1}\dot{\boldsymbol{p}}_u \otimes \boldsymbol{J}_v\big] \in \mathbb{C}^{MN\times P^2}$.

Moreover, the third term in (51) becomes

$$\begin{aligned}\boldsymbol{B}\dot{\hat{\boldsymbol{p}}}_v\Delta v &= \left(\sum_{i=0}^{P-1}\boldsymbol{D}_i \otimes a\boldsymbol{C}_{i+1}\right)\big(\boldsymbol{p}_u \otimes \dot{\boldsymbol{p}}_v\big)\Delta v \\ &= \left(\sum_{i=0}^{P-1}(\boldsymbol{D}_i \otimes \dot{\boldsymbol{J}}_v)(\boldsymbol{p}_u \otimes \bar{\boldsymbol{b}}_{i+1})\right)\Delta v \\ &= \hat{\boldsymbol{H}}\boldsymbol{b}\Delta v, \end{aligned} \tag{54}$$

where

- $\hat{\boldsymbol{H}} = \left[\boldsymbol{D}_0\boldsymbol{p}_u \otimes \dot{\boldsymbol{J}}_v, \boldsymbol{D}_1\boldsymbol{p}_u \otimes \dot{\boldsymbol{J}}_v, \ldots, \boldsymbol{D}_{P-1}\boldsymbol{p}_u \otimes \dot{\boldsymbol{J}}_v\right] \in \mathbb{C}^{MN\times P^2}$;
- $\dot{\boldsymbol{J}}_v = [\dot{\boldsymbol{p}}_v, \boldsymbol{J}_1\dot{\boldsymbol{p}}_v, \ldots, \boldsymbol{J}_{P-1}\dot{\boldsymbol{p}}_v] \in \mathbb{C}^{N\times P}$.

Hence, by substituting (52)-(54) into (51), it yields

$$\begin{aligned} a\boldsymbol{p}_{am}(\Delta u, \Delta v) &= \boldsymbol{H}_0\boldsymbol{b} + \tilde{\boldsymbol{H}}\boldsymbol{b}\Delta u + \hat{\boldsymbol{H}}\boldsymbol{b}\Delta v \\ &= \boldsymbol{H}(\Delta u, \Delta v)\boldsymbol{b} \end{aligned} \tag{55}$$

with $\boldsymbol{H}(\Delta u, \Delta v) = \boldsymbol{H}_0 + \tilde{\boldsymbol{H}}\Delta u + \hat{\boldsymbol{H}}\Delta v \in \mathbb{C}^{MN\times P^2}$.

C. Proof of Strict Concavity of the Objective Function in (27)

The existence of the global maximizer of (27) is guaranteed by the Weierstrass theorem [50], being the objective function in (27) continuous and the feasible set $\mathcal{S}$ non-empty and compact. It is also worth noting that the Hessian matrix of the objective function in (27) w.r.t. $\boldsymbol{\Delta\theta}$ can be calculated as $\boldsymbol{H}_{\rm e} = -2\hat{\boldsymbol{H}}_{\rm e}$ with $\hat{\boldsymbol{H}}_{\rm e}$ given by

$$\hat{\boldsymbol{H}}_{\rm e} = \begin{bmatrix} \boldsymbol{y}_A^\dagger\tilde{\boldsymbol{H}}_w^\dagger\tilde{\boldsymbol{H}}_w\boldsymbol{y}_A & \mathrm{Re}\{\boldsymbol{y}_A^\dagger\tilde{\boldsymbol{H}}_w^\dagger\hat{\boldsymbol{H}}_w\boldsymbol{y}_A\} \\ \mathrm{Re}\{\boldsymbol{y}_A^\dagger\tilde{\boldsymbol{H}}_w^\dagger\hat{\boldsymbol{H}}_w\boldsymbol{y}_A\} & \boldsymbol{y}_A^\dagger\hat{\boldsymbol{H}}_w^\dagger\hat{\boldsymbol{H}}_w\boldsymbol{y}_A \end{bmatrix}, \tag{56}$$

where $\tilde{\boldsymbol{H}}_w = \boldsymbol{S}^{-1/2}\tilde{\boldsymbol{H}}$, $\hat{\boldsymbol{H}}_w = \boldsymbol{S}^{-1/2}\hat{\boldsymbol{H}}$, and $\boldsymbol{y}_A = (\boldsymbol{A}_0^{(h-1)})^{-1}\boldsymbol{y}_0^{(h-1)} \in \mathbb{C}^{P^2}$. Then, the determinant of $\hat{\boldsymbol{H}}_{\rm e}$ is calculated as

$$\begin{aligned} |\hat{\boldsymbol{H}}_{\rm e}| &= \left(\boldsymbol{y}_A^\dagger\tilde{\boldsymbol{H}}_w^\dagger\tilde{\boldsymbol{H}}_w\boldsymbol{y}_A\right)\left(\boldsymbol{y}_A^\dagger\hat{\boldsymbol{H}}_w^\dagger\hat{\boldsymbol{H}}_w\boldsymbol{y}_A\right) \\ &\quad - \mathrm{Re}^2\left\{\boldsymbol{y}_A^\dagger\tilde{\boldsymbol{H}}_w^\dagger\hat{\boldsymbol{H}}_w\boldsymbol{y}_A\right\} \\ &> \left|\boldsymbol{y}_A^\dagger\tilde{\boldsymbol{H}}_w^\dagger\hat{\boldsymbol{H}}_w\boldsymbol{y}_A\right|^2 - \mathrm{Re}^2\left\{\boldsymbol{y}_A^\dagger\tilde{\boldsymbol{H}}_w^\dagger\hat{\boldsymbol{H}}_w\boldsymbol{y}_A\right\} \geq 0, \end{aligned} \tag{57}$$

where the first inequality holds for the Cauchy-Schwarz inequality[7] applied to the first term. Hence, $\boldsymbol{H}_{\rm e} \prec 0$, indicating that $g_a(\boldsymbol{\Delta\theta}|\boldsymbol{\Delta\theta}^{\star(h-1)})$ is strictly concave in $\boldsymbol{\Delta\theta}$.

D. Proof of Proposition 1

Proof: Let us define for simplicity:

- $g_a = g_a(\boldsymbol{y}, \boldsymbol{A}|\boldsymbol{y}_0^{(h-1)}, \boldsymbol{A}_0^{(h-1)})$;
- $\nabla_{\boldsymbol{A}} = \nabla_{\boldsymbol{A}} g(\boldsymbol{y}_0^{(h-1)}, \boldsymbol{A}_0^{(h-1)}) = -\boldsymbol{y}_A\boldsymbol{y}_A^\dagger$;
- $\nabla_{\boldsymbol{y}} = \nabla_{\boldsymbol{y}} g(\boldsymbol{y}_0^{(h-1)}, \boldsymbol{A}_0^{(h-1)}) = \boldsymbol{y}_A$,

then according to the first order optimality conditions, the optimal points can be obtained by forcing the gradient of g_a w.r.t. Δu and Δv to be zero, i.e., $\frac{\partial g_a}{\partial \Delta u} = 0$ and $\frac{\partial g_a}{\partial \Delta v} = 0$, which yields

$$\begin{aligned} 2\,\mathrm{Re}\left\{\nabla_{\boldsymbol{y}}^\dagger\frac{\partial \boldsymbol{y}}{\partial \Delta u}\right\} + \mathrm{tr}\left\{\nabla_{\boldsymbol{A}}\frac{\partial \boldsymbol{A}(\boldsymbol{\Delta\theta})}{\partial \Delta u}\right\} = 0, \\ 2\,\mathrm{Re}\left\{\nabla_{\boldsymbol{y}}^\dagger\frac{\partial \boldsymbol{y}(\boldsymbol{\Delta\theta})}{\partial \Delta v}\right\} + \mathrm{tr}\left\{\nabla_{\boldsymbol{A}}\frac{\partial \boldsymbol{A}(\boldsymbol{\Delta\theta})}{\partial \Delta v}\right\} = 0, \end{aligned} \tag{58}$$

with

- $\frac{\partial \boldsymbol{y}(\boldsymbol{\Delta\theta})}{\partial \Delta u} = \tilde{\boldsymbol{H}}_w^\dagger\boldsymbol{r}_w$ and $\tilde{\boldsymbol{H}}_w = \boldsymbol{S}^{-1/2}\tilde{\boldsymbol{H}}$;
- $\frac{\partial \boldsymbol{y}(\boldsymbol{\Delta\theta})}{\partial \Delta v} = \hat{\boldsymbol{H}}_w^\dagger\boldsymbol{r}_w$ and $\hat{\boldsymbol{H}}_w = \boldsymbol{S}^{-1/2}\hat{\boldsymbol{H}}$;
- $\frac{\partial \boldsymbol{A}(\boldsymbol{\Delta\theta})}{\partial \Delta u} = (\tilde{\boldsymbol{H}}_w^\dagger\boldsymbol{H}_{0w} + \boldsymbol{H}_{0w}^\dagger\tilde{\boldsymbol{H}}_w) + 2\tilde{\boldsymbol{H}}_w^\dagger\tilde{\boldsymbol{H}}_w\Delta u + (\tilde{\boldsymbol{H}}_w^\dagger\hat{\boldsymbol{H}}_w + \hat{\boldsymbol{H}}_w^\dagger\tilde{\boldsymbol{H}}_w)\Delta v$;
- $\frac{\partial \boldsymbol{A}(\boldsymbol{\Delta\theta})}{\partial \Delta v} = (\hat{\boldsymbol{H}}_w^\dagger\boldsymbol{H}_{0w} + \boldsymbol{H}_{0w}^\dagger\hat{\boldsymbol{H}}_w) + 2\hat{\boldsymbol{H}}_w^\dagger\hat{\boldsymbol{H}}_w\Delta v + (\hat{\boldsymbol{H}}_w^\dagger\tilde{\boldsymbol{H}}_w + \tilde{\boldsymbol{H}}_w^\dagger\hat{\boldsymbol{H}}_w)\Delta u$.

After some calculations, (58) becomes

$$\begin{aligned} c_1 + c_2\Delta u + c_3\Delta v = 0 \\ d_1 + d_2\Delta u + d_3\Delta v = 0, \end{aligned} \tag{59}$$

where

- $c_1 = \mathrm{Re}\left\{\boldsymbol{y}_A^\dagger\tilde{\boldsymbol{H}}_w^\dagger\boldsymbol{r}_w - \boldsymbol{y}_A^\dagger\tilde{\boldsymbol{H}}_w^\dagger\boldsymbol{H}_{0w}\boldsymbol{y}_A\right\}$;
- $c_2 = -\boldsymbol{y}_A^\dagger\tilde{\boldsymbol{H}}_w^\dagger\tilde{\boldsymbol{H}}_w\boldsymbol{y}_A$;
- $c_3 = -\mathrm{Re}\left\{\boldsymbol{y}_A^\dagger\tilde{\boldsymbol{H}}_w^\dagger\hat{\boldsymbol{H}}_w\boldsymbol{y}_A\right\}$;
- $d_1 = \mathrm{Re}\left\{\boldsymbol{y}_A^\dagger\hat{\boldsymbol{H}}_w^\dagger\boldsymbol{r}_w - \boldsymbol{y}_A^\dagger\hat{\boldsymbol{H}}_w^\dagger\boldsymbol{H}_{0w}\boldsymbol{y}_A\right\}$;
- $d_2 = c_3$;
- $d_3 = -\boldsymbol{y}_A^\dagger\hat{\boldsymbol{H}}_w^\dagger\hat{\boldsymbol{H}}_w\boldsymbol{y}_A$.

Hence, a unique stationary point to (27) is obtained as

$$\Delta\boldsymbol{\theta}_1 = [\widetilde{\Delta u}, \widetilde{\Delta v}]^{\rm T}, \tag{60}$$

where

$$\widetilde{\Delta u} = \frac{c_1d_3 - c_3d_1}{c_3^2 - c_2d_3} \quad \text{and} \quad \widetilde{\Delta v} = \frac{c_1d_2 - c_2d_1}{c_2d_3 - c_3^2}.$$

Note that if $\Delta\boldsymbol{\theta}_1$ is feasible, then it is the global optimal solution to the optimization problem (27). Otherwise, the optimal solution can be found on the boundaries of the feasible set, $\mathcal{S}$, namely determining for each edge the corresponding maximizer.

Case A: Upper and lower edges ($\Delta v = \pm\beta$).

Letting $\boldsymbol{H}_{\pm\beta} = \boldsymbol{S}^{-1/2}\big(\boldsymbol{H}_0 + \hat{\boldsymbol{H}}(\pm\beta)\big)$, the optimization problem in (27) boils down to

$$\begin{aligned} \Delta u^{\star(h)} &= \arg\max_{\Delta u\in\mathcal{A}} \\ & g_a(\Delta u; \Delta v = \pm\beta|\boldsymbol{y}_0^{(h-1)}, \boldsymbol{A}_0^{(h-1)})\Big|_{\substack{\boldsymbol{y}_0^{(h-1)}=\boldsymbol{y}\left(\boldsymbol{\Delta\theta}^{\star(h-1)}\right) \\ \boldsymbol{A}_0^{(h-1)}=\boldsymbol{A}\left(\boldsymbol{\Delta\theta}^{\star(h-1)}\right)}}, \end{aligned} \tag{61}$$

whose objective function of (61) can be written as

$$a'\,\Delta u^2 + b'_{\pm\beta}\,\Delta u + c'_{\pm\beta}, \tag{62}$$

with

$$a' = -\boldsymbol{y}_A^\dagger\tilde{\boldsymbol{H}}_w^\dagger\tilde{\boldsymbol{H}}_w\boldsymbol{y}_A, \tag{63a}$$

$$b'_{\pm\beta} = 2\,\mathrm{Re}\left\{\boldsymbol{y}_A^\dagger\tilde{\boldsymbol{H}}_w\boldsymbol{r}_w - \boldsymbol{y}_A^\dagger\tilde{\boldsymbol{H}}_w^\dagger\boldsymbol{H}_{\pm\beta}\boldsymbol{y}_A\right\}, \tag{63b}$$

and $c'_{\pm\beta}$ the constant terms independent of Δu.

Since $a' = -\mathrm{tr}\left\{\boldsymbol{A}_0^{-1}\boldsymbol{y}_0\boldsymbol{y}_0^\dagger\boldsymbol{A}_0^{-1}\tilde{\boldsymbol{H}}_w^\dagger\tilde{\boldsymbol{H}}_w\right\} < 0$, (62) is a concave optimization problem, whose optimal solution is given by

$$\Delta u_\pm^* = \max(\min(-b'_{\pm\beta}/(2a'), \alpha), -\alpha), \tag{64}$$

leading to the candidate optimal solutions associated with the up and down edges, namely

$$\Delta\boldsymbol{\theta}_2 = [\Delta u_+^*, \beta] \tag{65}$$

and

$$\Delta\boldsymbol{\theta}_3 = [\Delta u_-^*, -\beta]. \tag{66}$$

[7]Note that the first inequality in (57) is strict as a direct consequence of the full rank assumption of $\boldsymbol{H}_1$, which entails $\tilde{\boldsymbol{H}}$ and $\hat{\boldsymbol{H}}$ being linearly independent.

Case B: Left and right edges *($\Delta u = \pm\alpha$).*

Similar to **Case A**, letting $\boldsymbol{H}_{\pm\alpha} = \boldsymbol{S}^{-1/2}\big(\boldsymbol{H}_0 + \tilde{\boldsymbol{H}}(\pm\alpha)\big)$, the optimization problem (27) is equivalent to

$$\Delta v^{\star(h)} = \arg\max_{\Delta v\in\mathcal{B}} g_a(\Delta v;\, \Delta u = \pm\alpha | \boldsymbol{y}_0^{(h-1)}, \boldsymbol{A}_0^{(h-1)})\Big|_{\substack{\boldsymbol{y}_0^{(h-1)}=\boldsymbol{y}\left(\Delta\boldsymbol{\theta}^{\star(h-1)}\right)\\ \boldsymbol{A}_0^{(h-1)}=\boldsymbol{A}\left(\Delta\boldsymbol{\theta}^{\star(h-1)}\right)}}, \tag{67}$$

whose optimal solution is given by

$$\Delta v_{\pm}^{*} = \max(\min(-b''_{\pm\alpha}/(2a''), \beta), -\beta) \tag{68}$$

with

$$a'' = -\boldsymbol{y}_A^{\dagger}\hat{\boldsymbol{H}}_w^{\dagger}\hat{\boldsymbol{H}}_w\boldsymbol{y}_A, \tag{69a}$$

$$b''_{\pm\alpha} = 2\,\mathrm{Re}\Big\{\boldsymbol{y}_A^{\dagger}\hat{\boldsymbol{H}}_w\boldsymbol{r}_w - \boldsymbol{y}_A^{\dagger}\hat{\boldsymbol{H}}_w^{\dagger}\boldsymbol{H}_{\pm\alpha}\boldsymbol{y}_A\Big\}. \tag{69b}$$

As a consequence, the candidate optimal solutions associated with the left and right edges are

$$\Delta\boldsymbol{\theta}_4 = [\alpha,\, \Delta v_{+}^{*}] \tag{70}$$

and

$$\Delta\boldsymbol{\theta}_5 = [-\alpha,\, \Delta v_{-}^{*}]. \tag{71}$$

■

REFERENCES

[1] A. Farina, *Antenna-Based Signal Processing Techniques for Radar Systems*. Norwood, MA, USA: Artech House, 1992.

[2] B. Friedlander and A. J. Weiss, "Direction finding in the presence of mutual coupling," *IEEE Trans. Antennas Propag.*, vol. 39, no. 3, pp. 273–284, Mar. 1991.

[3] B. C. Ng and C. M. S. See, "Maximum likelihood sensor array calibration," *IEEE Trans. Antennas Propag.*, vol. 44, no. 6, pp. 827–835, Jun. 1996.

[4] J. Liang, X. Zeng, W. Wang, and H. Chen, "L-shaped array-based elevation and azimuth direction finding in the presence of mutual coupling," *Signal Process.*, vol. 91, no. 5, pp. 1319–1328, May 2011.

[5] H. Singh, H. L. Sneha, and R. M. Jha, "Mutual coupling in phased arrays: A review," *Int. J. Antennas Propag.*, vol. 2013, pp. 1–23, Jan. 2013.

[6] H. Steyskal and J. S. Herd, "Mutual coupling compensation in small array antennas," *IEEE Trans. Antennas Propag.*, vol. 38, no. 12, pp. 1971–1975, Dec. 1990.

[7] B. Liao and S. Chan, "Adaptive beamforming for uniform linear arrays with unknown mutual coupling," *IEEE Antennas Wireless Propag. Lett.*, vol. 11, pp. 464–467, 2012.

[8] T. Svantesson, "The effects of mutual coupling using a linear array of thin dipoles of finite length," in *Proc. 9th IEEE Signal Process. Workshop Stat. Signal Array Process.*, Jun. 1998, pp. 232–235.

[9] B. Friedlander, "Antenna array manifolds for high-resolution direction finding," *IEEE Trans. Signal Process.*, vol. 66, no. 4, pp. 923–932, Feb. 2018.

[10] M. Wax and J. Sheinvald, "Direction finding of coherent signals via spatial smoothing for uniform circular arrays," *IEEE Trans. Antennas Propag.*, vol. 42, no. 5, pp. 613–620, May 1994.

[11] I. Gupta and A. Ksienski, "Effect of mutual coupling on the performance of adaptive arrays," *IEEE Trans. Antennas Propag.*, vol. AP-31, no. 5, pp. 785–791, Sep. 1983.

[12] Z. Ye and C. Liu, "Non-sensitive adaptive beamforming against mutual coupling," *IET Signal Process.*, vol. 3, no. 1, pp. 1–6, Jan. 2009.

[13] A. Aubry, A. De Maio, L. Lan, and M. Rosamilia, "Adaptive radar detection and bearing estimation in the presence of unknown mutual coupling," 2022, *arXiv:2212.04261*.

[14] A. M. Elbir, "Direction finding in the presence of direction-dependent mutual coupling," *IEEE Antennas Wireless Propag. Lett.*, vol. 16, pp. 1541–1544, 2017.

[15] H. B. Li, Y. D. Guo, J. Gong, and J. Jiang, "Mutual coupling self-calibration algorithm for uniform linear array based on ESPRIT," in *Proc. 2nd Int. Conf. Consum. Electron., Commun. Netw. (CECNet)*, Apr. 2012, pp. 3323–3326.

[16] F. Sellone and A. Serra, "A novel online mutual coupling compensation algorithm for uniform and linear arrays," *IEEE Trans. Signal Process.*, vol. 55, no. 2, pp. 560–573, Feb. 2007.

[17] B. Liao, Z.-G. Zhang, and S.-C. Chan, "DOA estimation and tracking of ULAs with mutual coupling," *IEEE Trans. Aerosp. Electron. Syst.*, vol. 48, no. 1, pp. 891–905, Jan. 2012.

[18] H. Wu, C. Hou, H. Chen, W. Liu, and Q. Wang, "Direction finding and mutual coupling estimation for uniform rectangular arrays," *Signal Process.*, vol. 117, pp. 61–68, Dec. 2015.

[19] O. Besson, "Adaptive detection with bounded steering vectors mismatch angle," *IEEE Trans. Signal Process.*, vol. 55, no. 4, pp. 1560–1564, Apr. 2007.

[20] E. J. Kelly, "An adaptive detection algorithm," *IEEE Trans. Aerosp. Electron. Syst.*, vol. AES-22, no. 2, pp. 115–127, Mar. 1986.

[21] S. Bose and A. O. Steinhardt, "A maximal invariant framework for adaptive detection with structured and unstructured covariance matrices," *IEEE Trans. Signal Process.*, vol. 43, no. 9, pp. 2164–2175, Sep. 1995.

[22] H. L. Van Trees, *Optimum Array Processing: Part IV, Detection, Estimation, and Modulation Theory*. Hoboken, NJ, USA: Wiley, 2004.

[23] D. Ciuonzo, A. De Maio, and D. Orlando, "A unifying framework for adaptive radar detection in homogeneous plus structured interference—Part I: On the maximal invariant statistic," *IEEE Trans. Signal Process.*, vol. 64, no. 11, pp. 2894–2906, Jun. 2016.

[24] W. Liu, J. Liu, C. Hao, Y. Gao, and Y.-L. Wang, "Multichannel adaptive signal detection: Basic theory and literature review," *Sci. China Inf. Sci.*, vol. 65, no. 2, pp. 1–40, Feb. 2022.

[25] A. S. Paine, "Minimum variance monopulse technique for an adaptive phased array radar," *IEE Proc.-Radar, Sonar Navigat.*, vol. 145, no. 6, p. 374, 1998.

[26] U. Nickel, "Overview of generalized monopulse estimation," *IEEE Aerosp. Electron. Syst. Mag.*, vol. 21, no. 6, pp. 27–56, Jun. 2006.

[27] M. Greco, F. Gini, and A. Farina, "Joint use of sum and delta channels for multiple radar target DOA estimation," *IEEE Trans. Aerosp. Electron. Syst.*, vol. 43, no. 3, pp. 1146–1154, Jul. 2007.

[28] W. D. Blair and M. Brandt-Pearce, "Monopulse DOA estimation of two unresolved Rayleigh targets," *IEEE Trans. Aerosp. Electron. Syst.*, vol. 37, no. 2, pp. 452–469, Apr. 2001.

[29] A. Aubry, A. De Maio, S. Marano, and M. Rosamilia, "Single-pulse simultaneous target detection and angle estimation in a multichannel phased array radar," *IEEE Trans. Signal Process.*, vol. 68, pp. 6649–6664, 2020.

[30] S. M. Kay, *Fundamentals of Statistical Signal Processing: Detection theory* (Prentice Hall Signal Processing Series). Upper Saddle River, NJ, USA: Prentice-Hall, 1998.

[31] A. De Maio and M. Greco, *Modern Radar Detection Theory*. London, U.K.: IET, 2015.

[32] S. M. Kay, "The multifamily likelihood ratio test for multiple signal model detection," *IEEE Signal Process. Lett.*, vol. 12, no. 5, pp. 369–371, May 2005.

[33] Z. Ye and C. Liu, "On the resiliency of MUSIC direction finding against antenna sensor coupling," *IEEE Trans. Antennas Propag.*, vol. 56, no. 2, pp. 371–380, Feb. 2008.

[34] Y. Fang, S. Zhu, Y. Gao, L. Lan, C. Zeng, and Z. Liu, "Direction-of-arrival estimation of coherent signals for uniform linear antenna arrays with mutual coupling in unknown nonuniform noise," *IEEE Trans. Veh. Technol.*, vol. 71, no. 2, pp. 1656–1668, Feb. 2022.

[35] T. Svantesson, "Direction finding in the presence of mutual coupling," Chalmers Univ. Technol., Tech. Rep. L, 1999, vol. 307, p. 1999. [Online]. Available: http://www.pcc.lth.se/publications/papers/1999/svante.pdf

[36] Q. Yuan, Q. Chen, and K. Sawaya, "Performance of adaptive array antenna with arbitrary geometry in the presence of mutual coupling," *IEEE Trans. Antennas Propag.*, vol. 54, no. 7, pp. 1991–1996, Jul. 2006.

[37] J. Wu, F. Wen, and J. Shi, "Direction finding in bistatic MIMO radar with direction-dependent mutual coupling," *IEEE Commun. Lett.*, vol. 25, no. 7, pp. 2231–2234, Jul. 2021.

[38] J. Wu, F. Wen, and J. Shi, "Fast angle estimation in MIMO system with direction-dependent mutual coupling," *IEEE Commun. Lett.*, vol. 25, no. 9, pp. 2913–2917, Sep. 2021.

[39] R. A. Horn and C. R. Johnson, *Matrix Analysis*. Cambridge, U.K.: Cambridge Univ. Press, 1990.

[40] T. T. Wu and K. Lange, "The MM alternative to EM," *Stat. Sci.*, vol. 25, no. 4, pp. 492–505, Nov. 2010.

[41] J. M. Ortega and W. C. Rheinboldt, *Iterative Solution of Nonlinear Equations in Several Variables*, vol. 30. New York, NY, USA: Academic, 1970.
[42] W. J. Heiser, "Convergent computation by iterative majorization: Theory and applications in multidimensional data analysis," in *Advances in Descriptive Multivariate Analysis*, W. J. Krzanowski, Ed. Oxford, U.K.: Oxford Univ. Press, 1995, pp. 157–189.
[43] Y. Sun, P. Babu, and D. P. Palomar, "Majorization-minimization algorithms in signal processing, communications, and machine learning," *IEEE Trans. Signal Process.*, vol. 65, no. 3, pp. 794–816, Feb. 2017.
[44] M. Razaviyayn, M. Hong, and Z.-Q. Luo, "A unified convergence analysis of block successive minimization methods for nonsmooth optimization," *SIAM J. Optim.*, vol. 23, no. 2, pp. 1126–1153, Jan. 2013.
[45] A. Aubry, A. De Maio, A. Zappone, M. Razaviyayn, and Z. Luo, "A new sequential optimization procedure and its applications to resource allocation for wireless systems," *IEEE Trans. Signal Process.*, vol. 66, no. 24, pp. 6518–6533, Dec. 2018.
[46] S. Kraut, L. L. Scharf, and L. T. McWhorter, "Adaptive subspace detectors," *IEEE Trans. Signal Process.*, vol. 49, no. 1, pp. 1–16, Jan. 2001.
[47] M. A. Richards, *Principles of Modern Radar: Advanced Techniques*. Rijeka, Croatia: SciTech, 2010.
[48] F. C. Robey, D. R. Fuhrmann, E. J. Kelly, and R. Nitzberg, "A CFAR adaptive matched filter detector," *IEEE Trans. Aerosp. Electron. Syst.*, vol. 28, no. 1, pp. 208–216, Jan. 1992.
[49] A. Aubry, A. De Maio, and A. Farina, "Polarimetric radar signal processing," in *Radar, Sonar and Navigation*. Edison, NJ, USA: IET, 2022.
[50] D. P. Bertsekas, *Nonlinear Programming*. Belmont, MA, USA: Athena Scientific, 1999.

Lan Lan (Member, IEEE) was born in Xi'an, China, in 1993. She received the B.S. degree in electronic engineering and the Ph.D. degree in signal and information processing from Xidian University, Xi'an, in 2015 and 2020, respectively.

From July 2019 to July 2020, she was a Visiting Ph.D. Student with the University of Naples Federico II, Naples, Italy. She is currently an Associate Professor with the National Key Laboratory of Radar Signal Processing, Xidian University. Her research interests include frequency diverse array radar systems, MIMO radar signal processing, target detection, and ECCM. She was elected as the Youth Elite Scientist Sponsorship Program by the China Association for Science and Technology in 2022. She was a recipient of the URSI Young Scientists Awards in 2023 and the Excellent Paper Award from the CIE 2016 International Conference on Radar. She is currently on the editorial boards of *Digital Signal Processing*.

Massimo Rosamilia (Member, IEEE) received the B.S. (Hons.) and M.S. degrees in computer engineering from the University of Salerno, Fisciano, Italy, in 2017 and 2019, respectively, and the Ph.D. degree (cum laude) in information technologies and electrical engineering from the University of Naples Federico II, Naples, Italy, in 2023. From September 2021 to November 2021, he was a Visiting Ph.D. Student with Cranfield University, Shrivenham, U.K. From September 2022 to December 2022, he was a Visiting Ph.D. Student with the University of Luxembourg, Luxembourg. His research interests include statistical signal processing, with emphasis on radar signal processing. He ranked second in the Student Contest of the first International Virtual School on Radar Signal Processing in 2020. He also coauthored the paper winning the SET Panel Best Paper Award (Young Scientist) from the NATO SET-319 Specialists' Meeting on New Mathematical Frontiers for Multi-Dimensional Radar Systems in 2023.

Augusto Aubry (Senior Member, IEEE) received the Dr.Eng. degree (Hons.) in telecommunication engineering and the Ph.D. degree in electronic and telecommunication engineering from the University of Naples Federico II, Naples, Italy, in 2007 and 2011, respectively. From February 2012 to April 2012, he was a Visiting Researcher with Hong Kong Baptist University, Hong Kong. He is currently an Associate Professor with the University of Naples Federico II. His research interests include statistical signal processing and optimization theory, with emphasis on MIMO communications and radar signal processing. He was a co-recipient of the 2013 Best Paper Award (entitled to B. Carlton) of the IEEE TRANSACTIONS ON AEROSPACE AND ELECTRONIC SYSTEMS with the contribution "Knowledge-Aided (Potentially Cognitive) Transmit Signal and Receive Filter Design in Signal-Dependent Clutter" and a recipient of the 2022 IEEE Fred Nathanson Memorial Award as the young (less than 40 years of age) AESS Radar Engineer 2022, with the following citation "For outstanding contributions to the application of modern optimization theory to radar waveform design and adaptive signal processing."

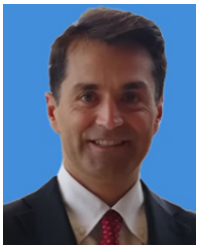

Antonio De Maio (Fellow, IEEE) received the Dr.Eng. (Hons.) and Ph.D. degrees in information engineering from the University of Naples Federico II, Naples, Italy, in 1998 and 2002, respectively. From October 2004 to December 2004, he was a Visiting Researcher with the U.S. Air Force Research Laboratory, Rome, NY, USA. From November 2007 to December 2007, he was a Visiting Researcher with The Chinese University of Hong Kong, Hong Kong. He is currently a Professor with the University of Naples Federico II. His research interests include the field of statistical signal processing, with emphasis on radar detection, optimization theory applied to radar signal processing, and multiple-access communications. He was a recipient of the 2010 IEEE Fred Nathanson Memorial Award as the young (less than 40 years of age) AESS Radar Engineer 2010 whose performance is particularly noteworthy as evidenced by contributions to the radar art over a period of several years, with the following citation for "robust CFAR detection, knowledge-based radar signal processing, and waveform design and diversity." He was a co-recipient of the 2013 Best Paper Award (entitled to B. Carlton) of the IEEE TRANSACTIONS ON AEROSPACE AND ELECTRONIC SYSTEMS with the contribution "Knowledge-Aided (Potentially Cognitive) Transmit Signal and Receive Filter Design in Signal-Dependent Clutter."

Guisheng Liao (Senior Member, IEEE) was born in Guilin, Guangxi, China, in 1963. He received the B.S. degree in mathematics from Guangxi University, Guangxi, in 1985, and the M.S. degree in computer science and the Ph.D. degree in electrical engineering from Xidian University, Xi'an, China, in 1990 and 1992, respectively.

From 1999 to 2000, he was a Senior Visiting Scholar with The Chinese University of Hong Kong, Hong Kong. He is currently a Yangtze River Scholars Distinguished Professor with the National Laboratory of Radar Signal Processing and serves as the Dean of the Hangzhou Institute of Technology, Xidian University. Since 2006, he has been serving as the panelists for the medium and long term development plan in high-resolution and remote sensing systems. Since 2007, he has been the Lead of Yangtze River Scholars Innovative Team and devoted in advanced techniques in signal and information processing. Since 2009, he has been an evaluation expert for the international cooperation project of Ministry of Science and Technology in China. His research interests include array signal processing, space-time adaptive processing, radar waveform design, and airborne/space surveillance and warning radar systems.

Open Access funding provided by 'Università degli Studi di Napoli "Federico II"' within the CRUI CARE Agreement